Supporting Information

Simultaneous generation of furfuryl alcohol, formate and H_2 by co-electrolysis of furfuryl and HCHO over bifunctional CuAg bimetallic electrocatalysts at ultra-low voltage

Liang Zhao [a], Zheng Lv [a], Yue Shi [a], Shuanglong Zhou [a], Yan Liu [a], Jiani Han [a], Qi Zhang [a], Jianping Lai [a] and Lei Wang [a,b*]*

[a] Key Laboratory of Eco-chemical Engineering, Ministry of Education, International Science and Technology Cooperation Base of Eco-chemical Engineering and Green Manufacturing, College of Chemistry and Molecular Engineering, Qingdao University of Science and Technology, Qingdao 266042, P.R. China.

[b] Shandong Engineering Research Center for Marine Environment Corrosion and Safety Protection, College of Environment and Safety Engineering, Qingdao University of Science and Technology, Qingdao 266042, P. R. China.

Chemicals and Materials. Cu foam, $Cu(NO_3)_2 \cdot 3H_2O$ (99%, Aladdin), $AgNO_3$ (99.99%, Sigma-Aldrich), Furfuryl (99.9%, Aladdin), Furfuryl alcohol (98%, Aladdin), HCHO (37%, Sigma-Aldrich), HCOOH (99%, Aladdin), HCl (37%, Aladdin), CH_3OH (99.5%, Aladdin), CH_3CH_2OH (99.5%, Aladdin), NaOH (96%, Aladdin), DMSO (99.9%, Aladdin), D_2O (99.9%, Aladdin). High pure Argon (99.999%) comes from Qingdao Deyi Gas Company. The deionized water (18 MΩ/cm) used in all experiments was prepared through ultrapure purification systems (Aqua Solutions).

Electrocatalysts Synthesis

Synthesis of Cu_xAg_y electrocatalysts on Cu foam (Cu_xAg_y/CF). To avoid the introduction of other metal compounds, copper foam (1.0 cm×1.5 cm) was used as a catalyst carrier. The copper foam was washed sequentially (10 min each time) with 1.0 M HCl, deionized water, and CH_3CH_2OH. Cu_x/Ag_y-CF was synthesized by electrodeposition on the CHI 660 electrochemical workstation, which uses a three-electrode configuration with a Pt sheet and an Ag/AgCl electrode as counter and reference electrode respectively. $Cu(NO_3)_2 \cdot 3H_2O$ (5 mM, 15 mM, 25 mM, 35 mM, 45 mM) and $AgNO_3$ (45 mM, 35 mM, 25 mM, 15 mM, 5 mM) were homogeneously mixed and dissolved in 20 mL of H_2O. Electrodeposition at -0.3 V vs. AgCl for 600 s. Synthesize a series of electrocatalysts: Cu_1Ag_9/CF, Cu_3Ag_7/CF, Cu_5Ag_5/CF, Cu_7Ag_3/CF and Cu_9Ag_1/CF.

Synthesis of Cu electrocatalysts on Cu foam (Cu/CF). $Cu(NO_3)_2 \cdot 3H_2O$ (25 mM) was dissolved in 20 mL of H_2O. All experimental steps were the same as above.

Synthesis of Ag electrocatalysts on Cu foam (Ag/CF). $AgNO_3$ (25 mM) was dissolved in 20 mL of H_2O. All experimental steps were the same as above.

Characterization. To study the morphology and structure of the catalyst, a Hitachi S-4800 scanning electron microscope (SEM) was tested. The morphology of the samples was characterized using transmission electron microscopy (TEM) and high resolution TEM (HRTEM) on a JEM-2100UHR with an accelerating voltage of 200 KV. X-ray diffraction (XRD) analysis at a scanning rate of $1°min^{-1}$ in the 2θ ranges from 5 to 90° was used to examine the composition of the as-synthesized samples on X'Pert PRO MPD diffractometer (Netherlands PANalytical) operating at 40 KV and 40 mA with Cu Kα radiation. X-ray photoelectron spectra (XPS) were collected using a VG ESCALABMK II spectrometer. All the electrochemical properties of the samples were performed on an electrochemical station (CHI 660E). The content of elements is determined by inductively coupled plasma atomic emission spectrometer (ICP-AES, Varian 710-ES). H_2 evaporated by an electrolytic process is quantified by gas chromatography (GC 7900) equipped with a thermal conductivity detector (TCD) and a flame ionization detector (FID) and using Ar (99.999%) as the carrier gas. ^1H NMR spectra were recorded on a BRUKER AVANCE NEO 400 MHz liquid NMR spectrometer in the indicated solvents.

Electrochemical Measurements. On the CHI660 electrochemical workstation (Shanghai Zhenhua Instrument Corporation, Shanghai, China), electrochemical measurements were made in the conventional three-electrode trough with platinum wire as the opposite electrode and Hg/HgO electrode as the reference electrode. All electrochemical measurements were converted to RHE. All potentials measured in 1.0 M KOH and 0.05 M FF solution or 1.0 M KOH and 0.6 M HCHO solution were converted to values about RHE according to the equation:

$$E(RHE) = E(SCE) + 0.2415\ V + 0.0592 \times pH.$$

FF and HCHO (37 wt%) solutions were used directly as reducing and oxidation substrate, respectively. In addition, linear sweep voltammetry (LSV) was conducted at a scan rate of 5 mV/s. Electrochemical double layer capacitance (C_{dl}) measurements were performed by cyclic voltammetry, collected at non-Faraday areas at different scan rates of 20 to 100 mV/s at potentials between 0.08 and 0.18 V vs. RHE in 1.0 M KOH and 0.05 MFF solution. Electrochemical impedance spectroscopy (EIS) was performed on the PAR-STAT 2273 test system with a frequency range of 100 kHz to 1 Hz with an AC signal amplitude of 10 mV, -0.3 V vs. RHE.

Two-electrode electrolysis was performed on an H-type electrochemical workstation with an anion exchange membrane. For the FOR/FEH two-electrode electrolytic cell, Cu_3Ag_7/CF was used for the anode and Cu_7Ag_3/CF for the cathode, including 1.0 M KOH and 0.6 M HCHO solution for the anode and 1.0 M KOH and 0.05 M FF solution for the cathode. Then, chronoamperometric tests were performed at different potentials, and Ar was continuously injected into the anode cell during the experiment. To analyze the gas products in the anode and cathode chambers, different cell voltages (from 0.3 to 0.7 V) were measured using Cu_3Ag_7/CF as the anode and Cu_7Ag_3/CF as the cathode in the two-electrode configuration. FE analysis of H_2, FA and FM production in the cathode and anode chambers was carried out from five consecutive 1 h controlled-current density electrolysis (500 mA cm^{-2}) using Cu_3Ag_7/CF and Cu_7Ag_3/CF couples, but with fresh electrolyte for each cycle.

Measurement of ECSA. To estimate ECSA values of the materials, double-layered capacitance (C_{dl}) was measured using a simple cyclic voltammetry method. The potential was selected beyond the possible Faraday area (0.08 ~ 0.18 V vs. RHE) of the material to record the CV at different scan rates of 20 ~ 100 mV/s. The capacitive current density ΔJ/2 was linearly correlated with the scan rate, and the double layer capacitance (C_{dl}) was calculated from the slope of these straight lines. Using standard specific capacitance values for 1.0 cm^{-2} surfaces (~0.04 mF), the C_{dl} was further converted to ECSA.

$$\mathrm{ECSA} = \frac{\mathrm{C_{dl}}}{\mathrm{C_s}}$$

$$\mathrm{C_s} = 0.04\ \mathrm{mF\ cm^{-2}}$$

Calculation of turnover frequency. Owing to the bulk nature of the catalysts, we selected an electrochemical method to obtain the TOF values of each sample. Nearly all the surface-active sites were assumed to be accessible by the electrolyte, and then the TOF values could be calculated by the following equation:

$$\mathrm{TOF} = \frac{\mathrm{I}}{4\mathrm{Fn}}$$

where *I*, *n*, and *F* are current during linear sweep measurement, the number of active site numbers, and the Faraday constant, respectively. The factor 1/4 is because electrolysis requires four electrons for the evolution of one hydrogen molecule from two protons and a FF from a FA. Value (n), calculated from the CV data from the RHE in the range -0.3 V to +0.6 V in 1 M phosphate buffer (pH=7.4), with a scan rate of

50 mV/s. Since it is difficult to attribute the observed peak to a specific redox dual, the surface active site is almost linear with the integrated voltammetric charge (cathode and anode) on the CV curve. Assuming a one-electron process for both reduction and oxidation, we can evaluate the upper limit of the active site number according to the follow formula:

$$n = \frac{Q_{cv}}{2F}$$

Product analysis. Gas products were analyzed using gas chromatography (GC 7900) equipped with a thermal conductivity detector (TCD) and flame ionization detector (FID). Argon (99.99%) was used as a carrier gas. The quantity of H_2 production was determined via a water displacement method.

Liquid aliquots (0.5 mL) were taken before and after the preparative electrolysis experiments, diluted twice with acetonitrile, and analyzed using high performance liquid chromatography (HPLC), which was carried out on an Agilent Infinity 1260 II HPLC system (Agilent Technologies) equipped with a 220 nm UV-vis detector. The aliquots were fed through a Zorbax SB C-18 column (4.6×50mm, 3.5-micron, Agilent Technologies). FF and FA were quantified using HPLC by producing calibration curves. The mobile phase was V (acetonitrile) : V (water) = 50:50 at a flow rate of 1.0 mL/min with a detection wavelength of 220 nm and a column temperature of 25℃. FF and FA could be completely separated within 4 min.

HCHO concentration during electrolysis was quantified by UV-vis absorption measurements after the Hanke reaction. Ammonium acetate (15.4 g) was placed in water (50 mL), glacial acetic acid (0.3 mL) and acetylacetone (0.2 mL) and mixed with stirring to form a solution that was further diluted with water (49.5 mL). To determine the concentration of HCHO, 20.0 μL of the electrolyte was acidified with 20 μL of 2.0 M HCl acid and then diluted 2500 times before and after electrolysis. Subsequently, 2.0 mL of the diluted solution was mixed with acetylacetone solution (2.0 mL) and further heated to 60°C for 10 min. after cooling for 10 min, the absorbance of the sample solution was measured at 413 nm. Quantification of HCHO was obtained from the calibration curve by applying a pure HCHO standard solution of known concentration.

The identification and quantification of formic acid and methanol were determined from ^{1}H NMR using a calibration curve with DMSO (10.0 mM) as an internal standard. Before and after electrolysis 500 μL of electrolyte was acidified by 20 μL of HCl (37%) and then added to 100 μL of D_2O. ^{1}H NMR was recorded using the water suppression method.

The Faradaic effificiency was calculated on the basis of the following equation:

$$\text{FE}\ (\%) = \frac{nF \times N}{Q_{\text{total charge passed}}} \times 100\ \%$$

where n is the number of electrons transferred for each product molecule, F is Faraday's constant (96,485 C mol^{-1}), N is the mole number of products and Q is the total passed charge.

FA conversion (%), product selectivity (%) and yield (%):

$$\text{Conversion (\%)} = \frac{\text{mole of furfural consumed}}{\text{mole of furfural initial}} \times 100\ \%$$

$$\text{Selectivity (\%)} = \frac{\text{mole of furfuryl alcohol formed}}{\text{mole of furfural consumed}} \times 100\ \%$$

$$\text{yield (\%)} = \frac{\text{mole of furfuryl alcohol formed}}{\text{mole of furfural initial}} \times 100\ \%$$

The carbon balance (%) of the electrooxidation process was calculated using the following equation:

$$\text{carbon balance (\%)} = \frac{\text{mol of organic products}}{\text{mol of formaldehyde consumed}} \times 100\ \%$$

The carbon balance (%) of the electroreduction process was calculated using the following equation:

$$\text{carbon balance (\%)} = \frac{n_{FF} + n_{FA}}{n^{o}_{FF}} \times 100\ \%$$

The n_{FF}, n_{FA} represents the mole amounts of FF and FA after the electrolysis. The n^{0}_{FF} represents the mole amount of FF before reaction.

In-Situ Fourier Transform Infrared Spectroscopy (FTIR) Technique. Operation process of silicon plane gold plating film: preparation of gold plating solution. Preparation solution A: dissolve 0.1222 g NaOH and 0.2286 g $NaAuCl_4 \cdot 2H_2O$ in 3 mL deionized water and dissolve by ultrasonic for 1 h: 0.134 g NH_4Cl, 0.9468 g Na_2SO_3 and 0.6202 g $Na_2S_2O_3 \cdot 5H_2O$ in 50 mL deionized water and sonicated for 1 h. Solution A was mixed with solution B, adding 50 mL of deionized water and fully sonicated for 2 h. Silicon crystal plating preparation: soak the silicon crystal in royal water (V (HCl): V (HNO_3) = 3:1) for 30 min, and then rinse with deionized water. Secondly, grind 50 μm Al_2O_3 powder on the electrode cloth in the clockwise direction of silicon crystal plating for 10 min, and then wash with deionized water. Third, deionized water and acetone were treated alternately 5 times, for 2 min, 1 min, 1 min, 1 min and 2 min respectively. Fourth, take out the oxidized solution (V (H_2SO_4): V (H_2O_2) = 3:1) and rinse with deionized water. Finally, the silicon coating was soaked in 40% NH_4F solution for 4-5 min and rinsed with deionized water. Gold film deposition: put 15 mL gold plating solution into a 25 mL beaker, preheat in a 50-55℃ water bath for 2 min, and then add 3.4 mL 2% HF. Secondly, the prepared silicon crystals were soaked in the above solution for 4-5 min, and finally washed with deionized water to obtain the gold plating layer.

In-Situ Raman Technique. The in situ Raman spectrum was obtained by using a specially designed electrolytic cell consisting of the bottom working electrode, platinum wire as the opposite electrode and the reference electrode. The electrode area was fixed to 1 cm^2. A 60X objective confocal Raman microscope (inVia Qontor, Renishaw) was used. The laser wavelength used in all experiments was 532 nm. The signal acquisition time is 90 s for each Raman spectrum.

AEM Electrolysis. Before use, degrease and pretreat in 0.1 M HCl solution to remove contaminants from the oxide layer on the instrument surface. Then, clip the anion exchange membrane (Sustainion X37-50) between the cathode and anode catalyst to build an electrolytic cell (Cu_3Ag_7/CF(+)||Cu_7Ag_3/CF(–)). At room temperature, the cathode electrolyte (1.0 M KOH and 0.05 M FF solution) and the anode electrolyte

(1.0 M KOH and 0.6 M HCHO solution) were continuously supplied to both sides of the electrolytic cell with a circulating pump at a flow rate of 60 mL/min.

Calculation Setup. The framework for density functional theory implemented in the VASP program. The generalzied gradient approximation proposed by Perdew, Burke, and Ernzerhof is selected for the exchange-correlation potential. The cut-off energy for plane wave is set to 500 eV. The energy criterion is set to 10−5 eV in iterative solution of the Kohn-Sham equation. For all models the vacuum space along the z-direction was set to be 15 Å, which was enough to avoid interaction between the two neighboring images. The Brillouin zone integration is performed using a 2×2×1 k-mesh. All the structures are relaxed until the residual forces on the atoms have declined to less than 0.02 eV/Å. The Van der Waals dispersion-corrected DFT was also carried out, as proposed by Grimme et al. The barriers for transition states are calculated with the climbing-image nudged elastic band (CI-NEB) method. The free energy (ΔG) for elemental reaction step were calculated as:

$$\Delta G = \Delta E + \Delta EZPE - T\Delta S$$

where ΔE is the difference between the total energy, ΔEZPE and ΔS are the differences in the zero-point energy and the change of entropy, T is the temperature (T = 300 K in this work), respectively.

Figures

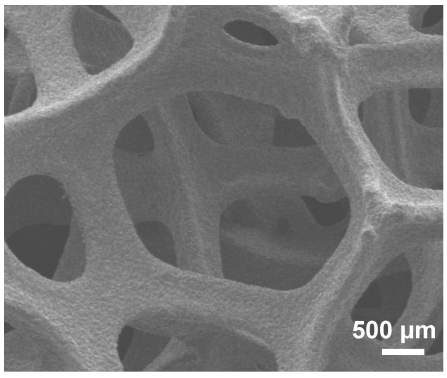

Figure S1. SEM image of treated copper foam.

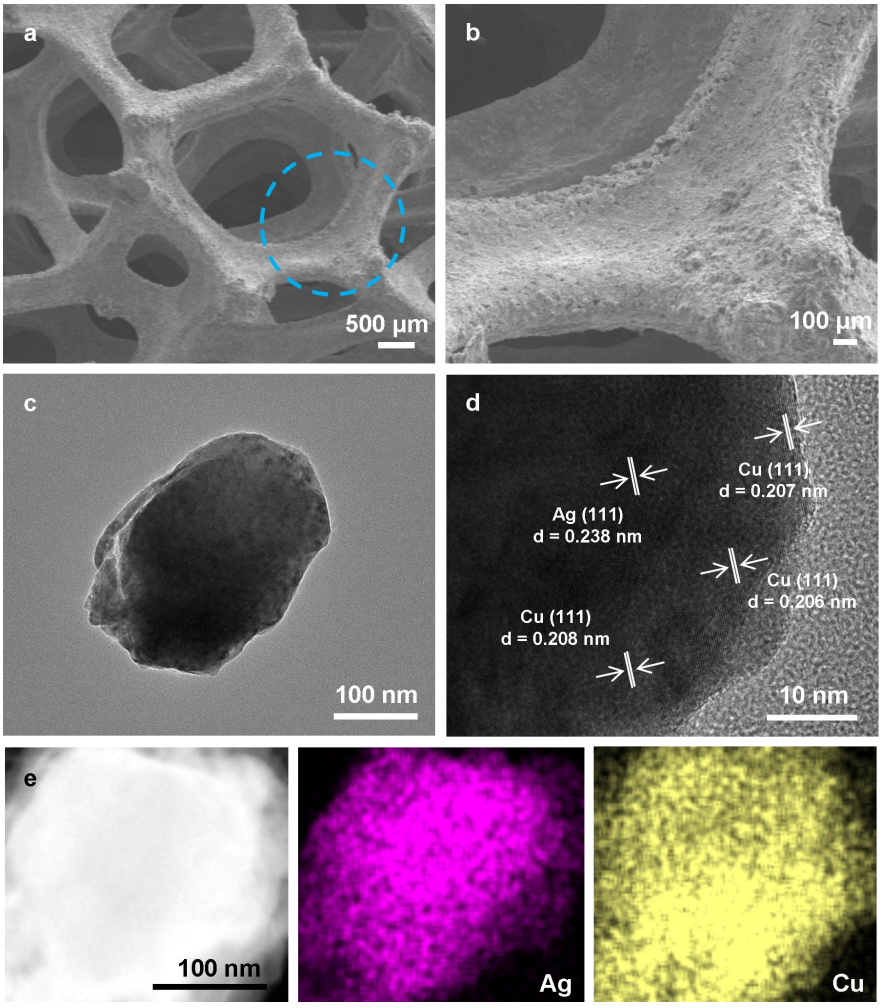

Figure S2. Morphology and elemental compositions of the Cu_3Ag_7/CF electrocatalysts. (a-b) SEM images. (c) TEM image. (d) HRTEM image. (e) STEM image and corresponding elemental mappings.

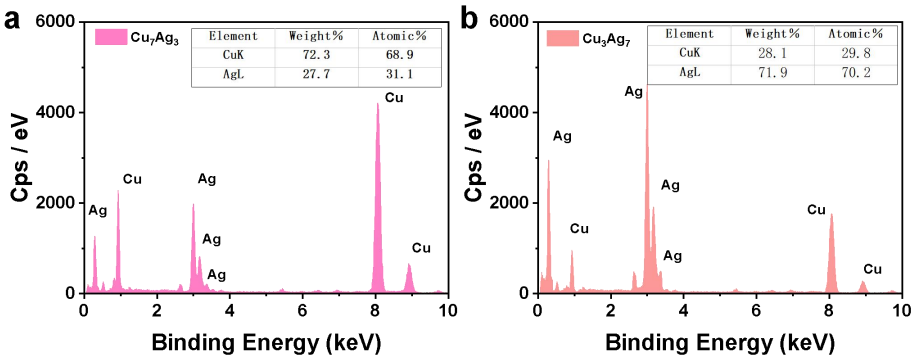

Figure S3. EDX spectroscopy analysis. (a) Cu_7Ag_3. (b) Cu_3Ag_7.

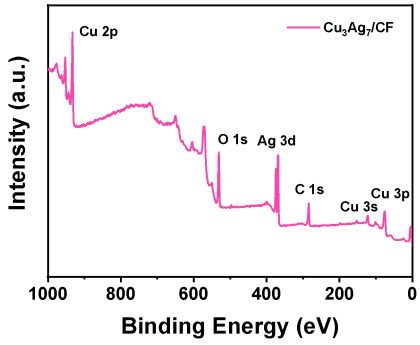

Figure S4. XPS survey spectra of Cu_3Ag_7/CF.

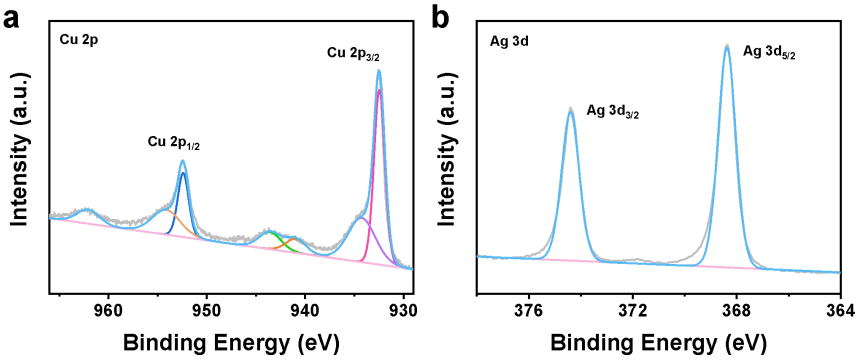

Figure S5. High-resolution XPS spectra of Cu_3Ag_7/CF. (a) Cu 2p. (b) Ag 3d.

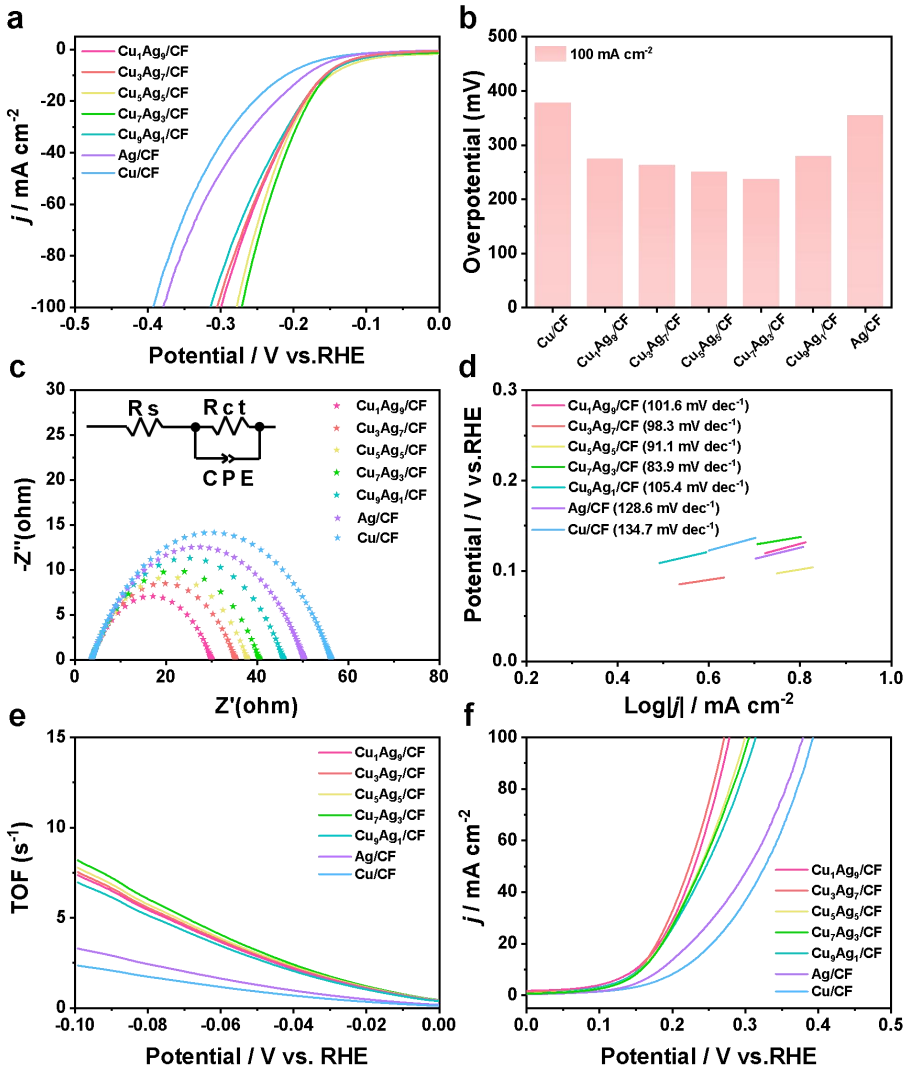

Figure S6. Electrochemical measurements of prepared catalysts. (a) LSV curves, (b) comparison of onset potentials at 100 mA cm^{-2}, (c) Nyquist plots, (d) Tafel slopes, (e) TOF curves in 1.0 M KOH and 0.05 M FF. (f) LSV curves in 1.0 M KOH and 0.6 M HCHO.

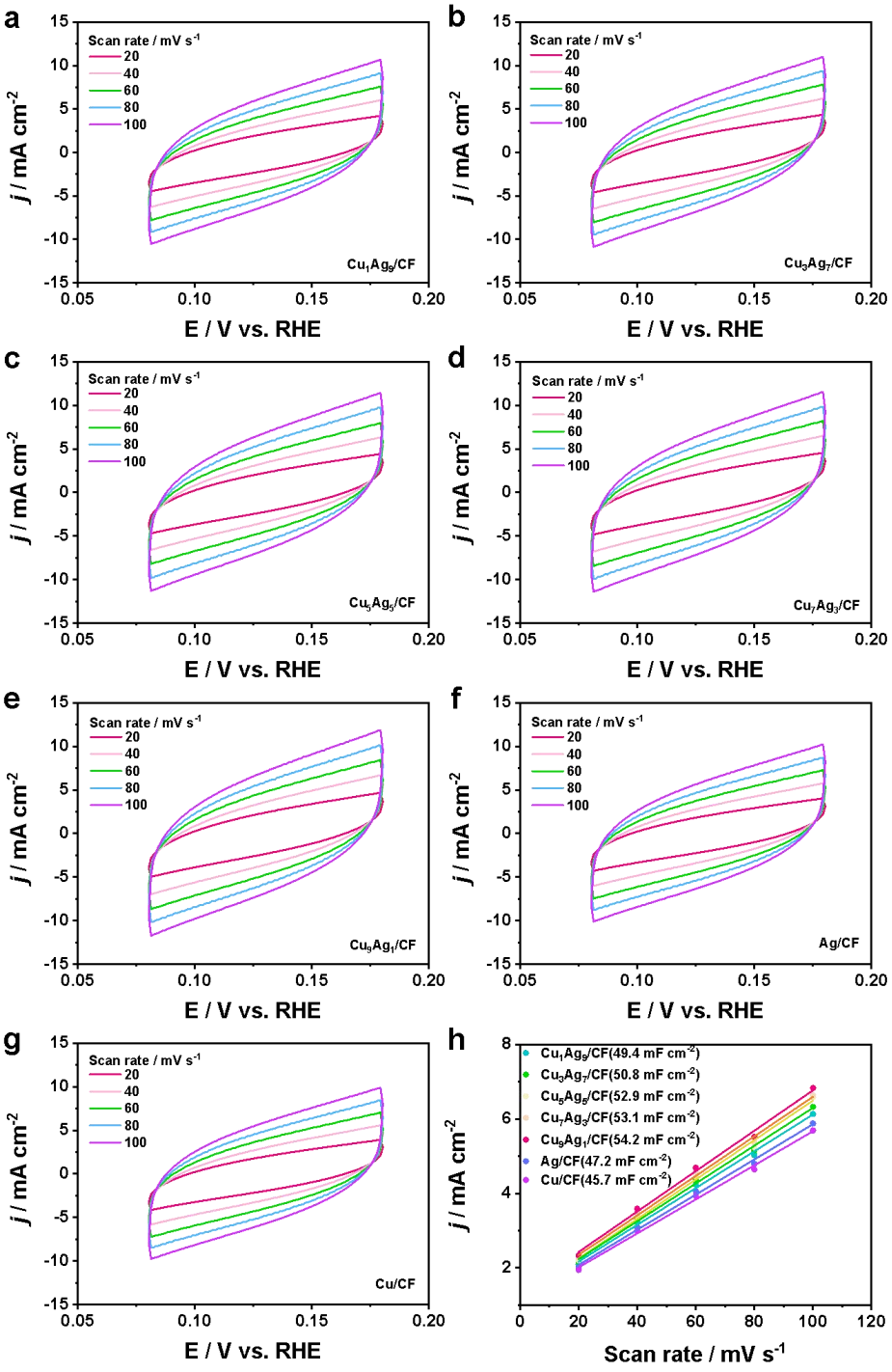

Figure S7. CV test. CV curves for the (a-e) Cu_xAg_y/CF, (f) Cu/CF , and (g) Ag/CF were collected in a non-Faradaic region with various scan rates ranging from 20 to 100 mV s^{-1} at potentials between 0.08 V and 0.18 V_{RHE} in 1.0 M KOH. h) C_{dl} values of Cu/CF, Ag/CF, and Cu_xAg_{10-x}/CF based on corresponding CV curves.

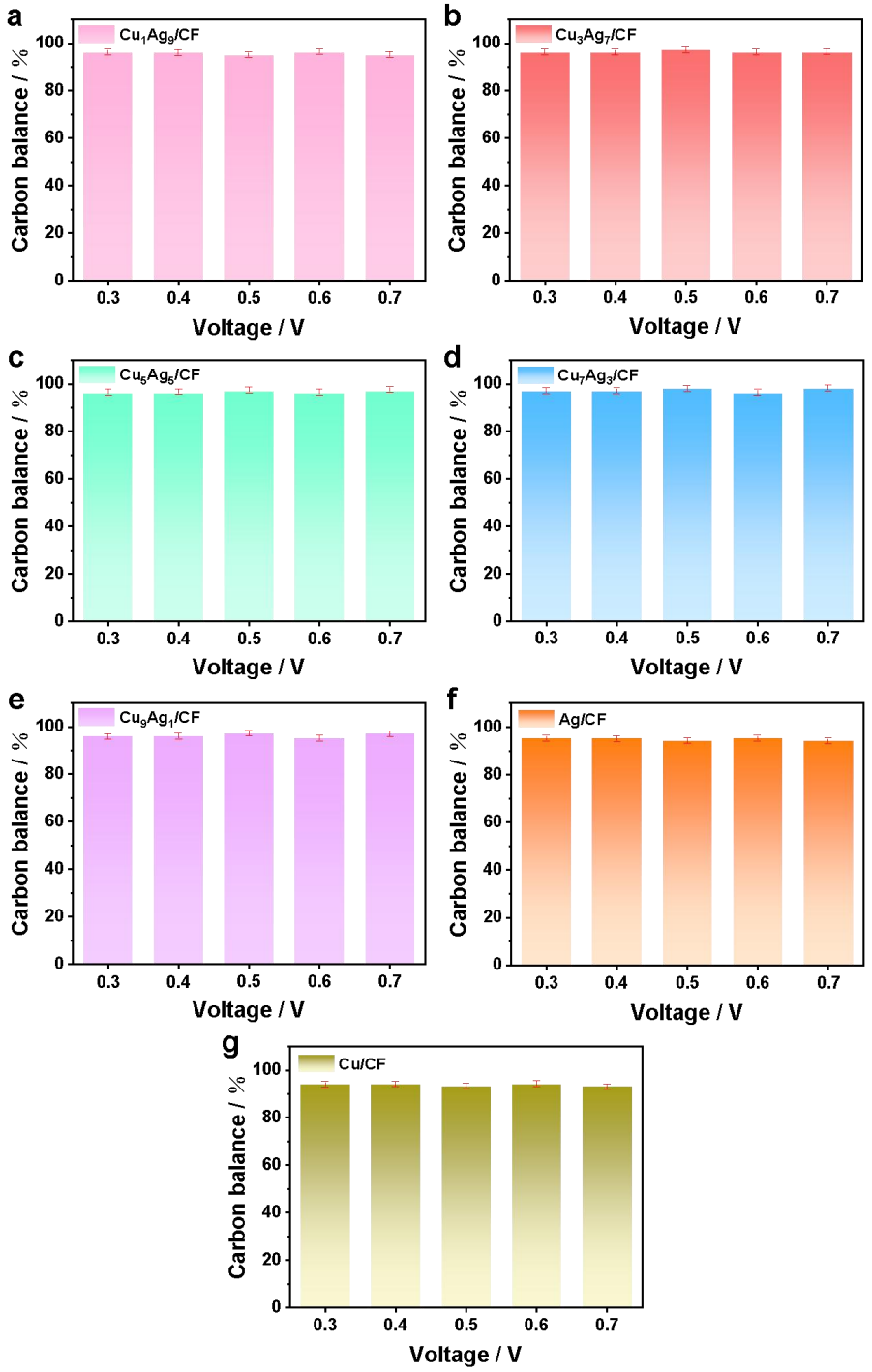

Figure S8. Carbon balance of FF electrolysis over different samples. (a) Cu_1Ag_9/CF, (b) Cu_3Ag_7/CF, (c) Cu_5Ag_5/CF, (d) Cu_7Ag_3/CF, (e) Cu_9Ag_1/CF, (f) Ag/CF, and (g) Cu/CF. Error bars represent the standard deviation from at least three independent measurements.

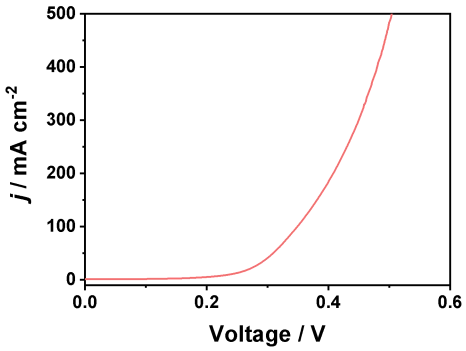

Figure S9. The two-electrode LSV curves for FOR/FEH. Cu_3Ag_7/CF and Cu_7Ag_3/CF were used as an anode and cathode, respectively. For anodic FEH, the solution was in 1.0 M KOH and 0.05 M FF; for anodic FOR, the solution was 1.0 M KOH and 0.6 M HCHO.

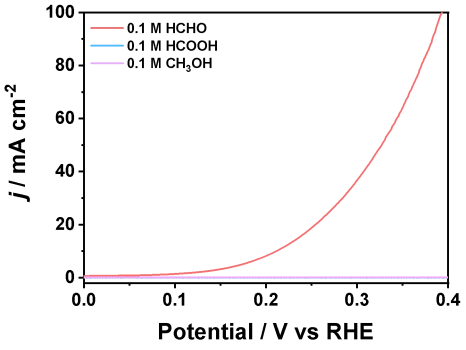

Figure S10. LSV curves for Cu_3Ag_7/CF after addition of 0.1 M HCOOH, 0.1 M CH_3OH and 0.1 M HCHO to 1.0 M KOH under Ar.

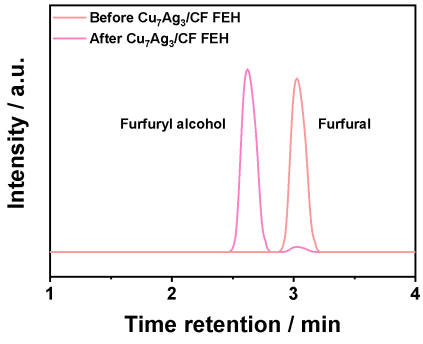

Figure S11. HPLC chromatogram of products before and after FEH for Cu_7Ag_3/CF at 0.5 V.

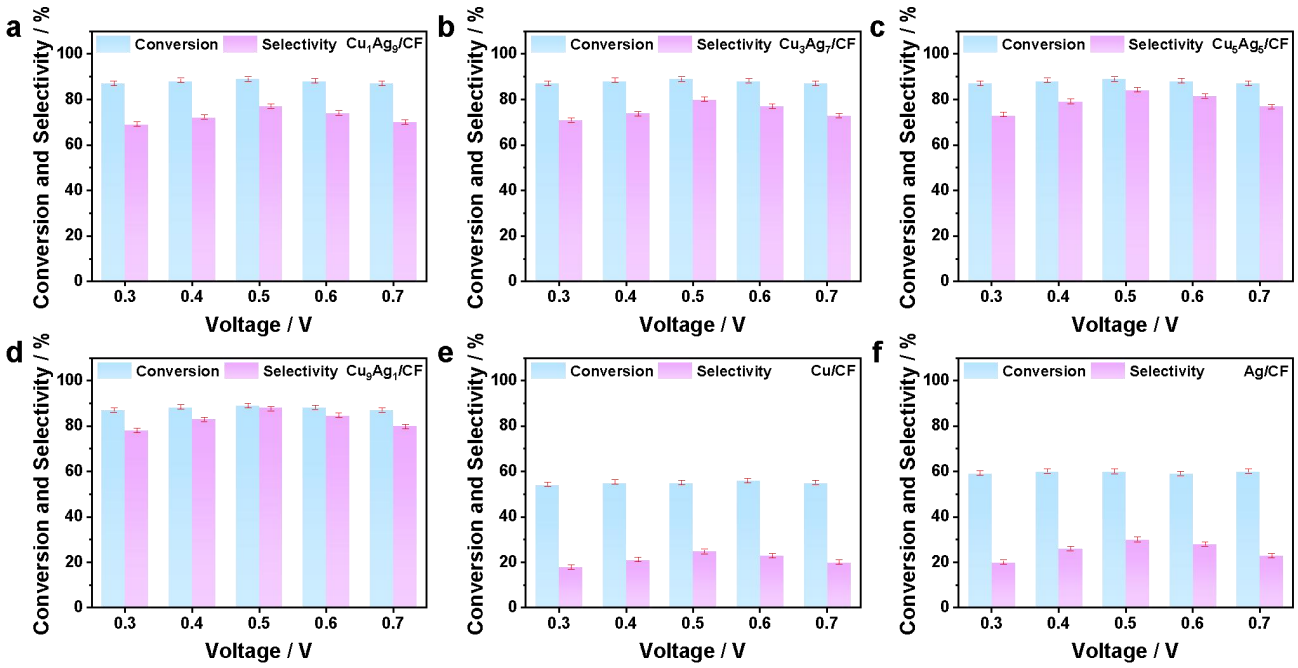

Figure S12. Conversion and selectivity of FEH for different samples. (a) Cu_1Ag_9/CF, (b) Cu_3Ag_7/CF, (c) Cu_5Ag_5/CF, (d) Cu_9Ag_1/CF, (e) Cu/CF and (f) Ag/CF. Error bars represent the standard deviation from at least three independent measurements.

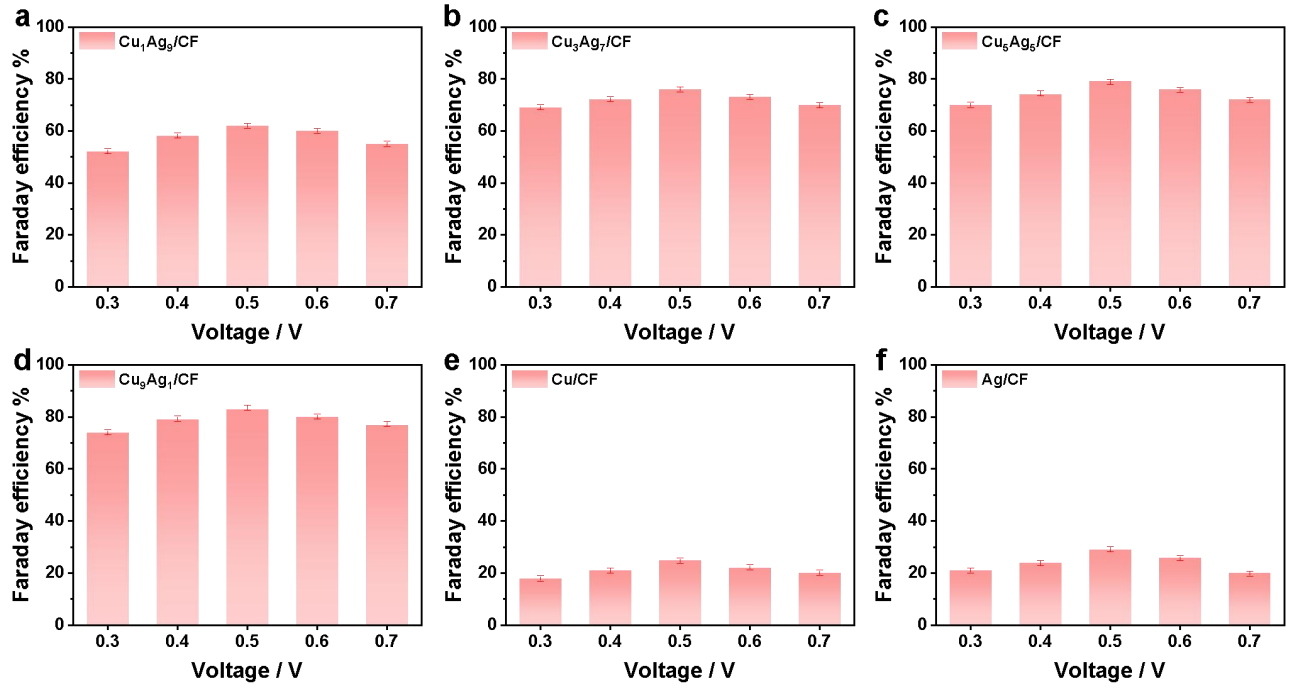

Figure S13. Faradaic efficiencies of FEH for different samples. (a) Cu_1Ag_9/CF, (b) Cu_3Ag_7/CF, (c) Cu_5Ag_5/CF, (d) Cu_9Ag_1/CF, (e) Cu/CF and (f) Ag/CF. Error bars represent the standard deviation from at least three independent measurements.

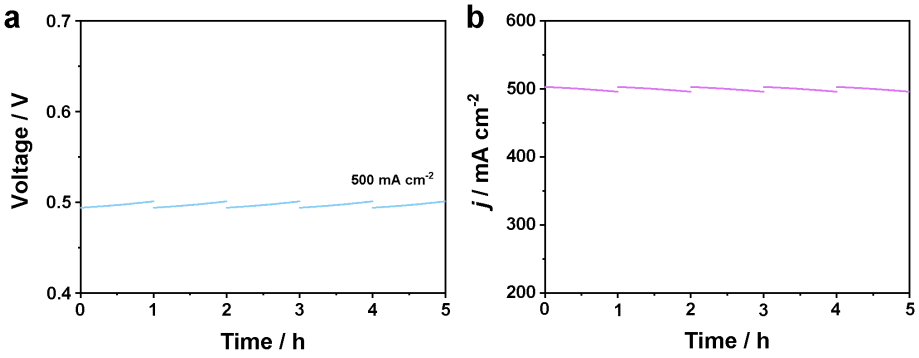

Figure S14. Stability testing of H-type cell. (a) Chronopotentiometric curves for five consecutive controlled-current density electrolysis cycles conducted at 500 mA cm^{-2}. (b) Fresh FF and HCHO were periodically replenished at a cell voltage of 0.5 V to bring it back to the original concentration of the solution.

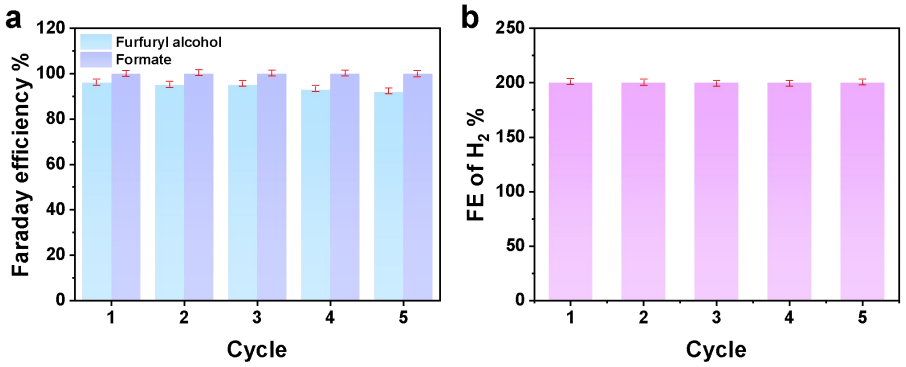

Figure S15. FE of (a) FA, FM and (b) H_2 production for five consecutive 1 h controlled-current density (500 mA cm^{-2}) electrolysis cycles. Error bars represent the standard deviation from at least three independent measurements.

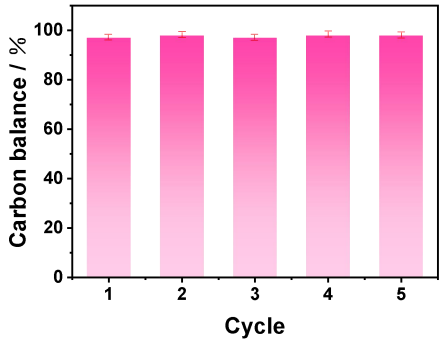

Figure S16. Carbon balance of FF reduction in per electrolysis cycle. Error bars represent the standard deviation of at least three independent measurements.

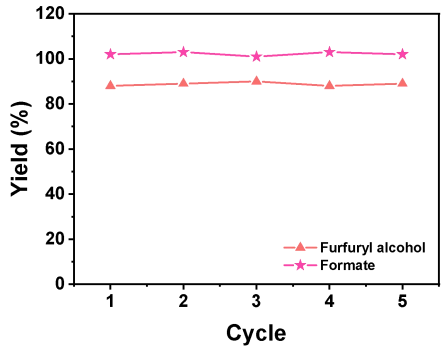

Figure S17. Yield of FA and formate production for five consecutive 1 h controlled-current density (500 mA cm^{-2}) electrolysis cycles.

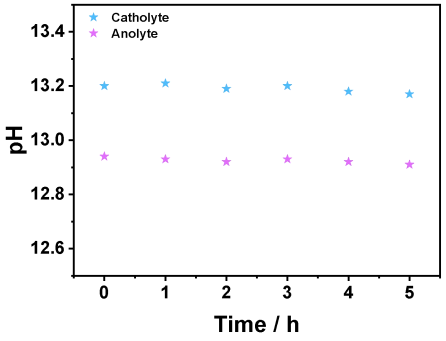

Figure S18. pH change of anolyte and catholyte during electrolysis in a continuous flow process. Electrolysis was performed in a two-electrode flow cell at a constant current of 500 mA using a Cu_3Ag_7/CF (anode) and Cu_7Ag_3/CF (cathode) electrocatalyst coupling. 1.0 M KOH and 0.05 M FF were used as the catholyte while 1.0 M KOH with 0.6 M HCHO as the anolyte. Flow rates of both anolyte and catholyte were set as 50 mL min^{-1}. Error bars represent the standard deviation from at least three independent measurements.

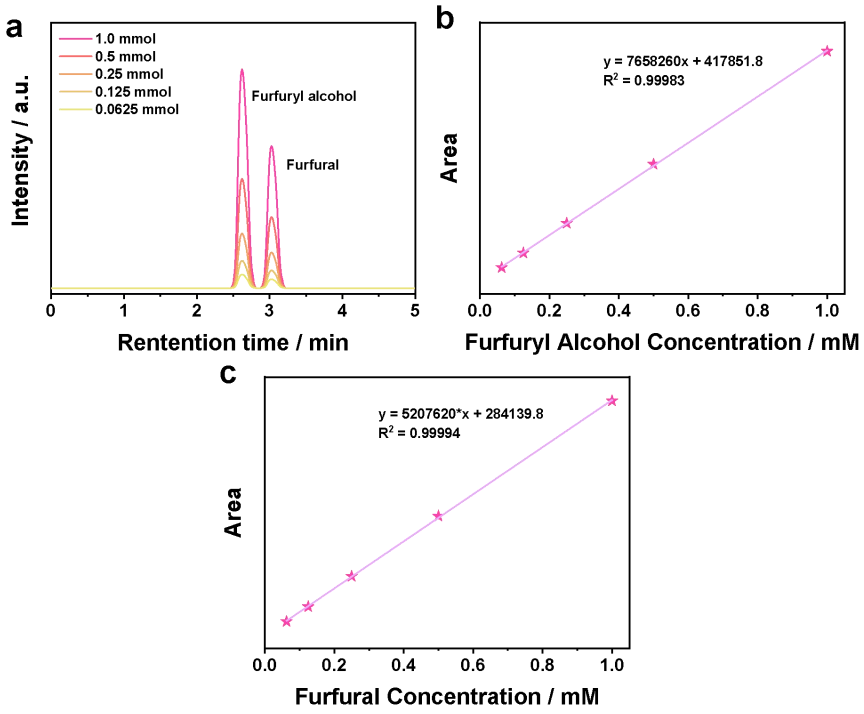

Figure S19. Calibration curves for the HPLC quantification of (a, b) FA and (a, c) FF.

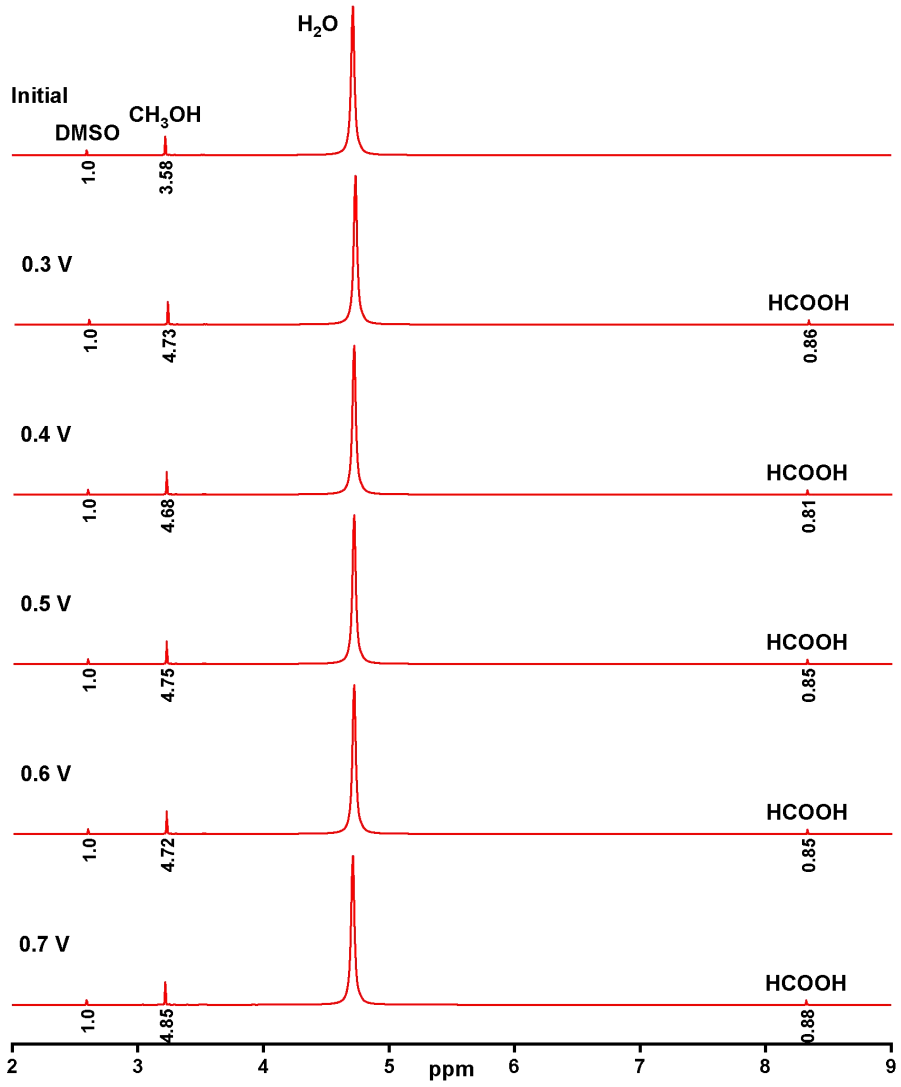

Figure S20. ^{1}H NMR (D_2O, 400 MHz) of organic products in the liquid phase of the anode chamber in a two-electrode electrolyzer using Cu_3Ag_7/CF and Cu_7Ag_3/CF pairings, electrolyzed at different voltages.

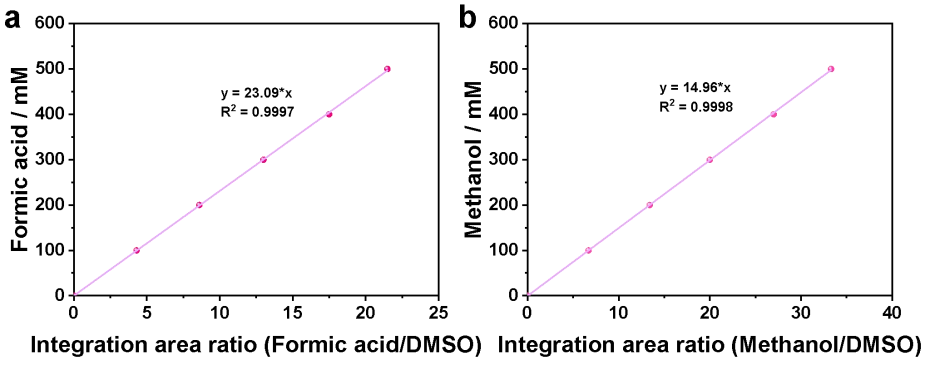

Figure S21. Calibration curves for the ^{1}H NMR quantification of (a) formic acid and (b) methanol using DMSO as an internal standard.

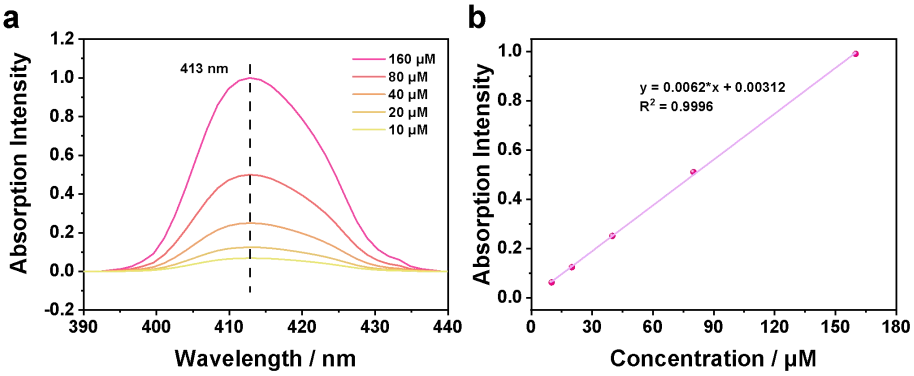

Figure S22. (a) UV-vis absorption spectra of the product from the reaction between acetyl acetone and HCHO of different concentrations. (b) Calibration curve obtained by plotting the HCHO concentration against absorption peak intensity at λ = 413 nm.

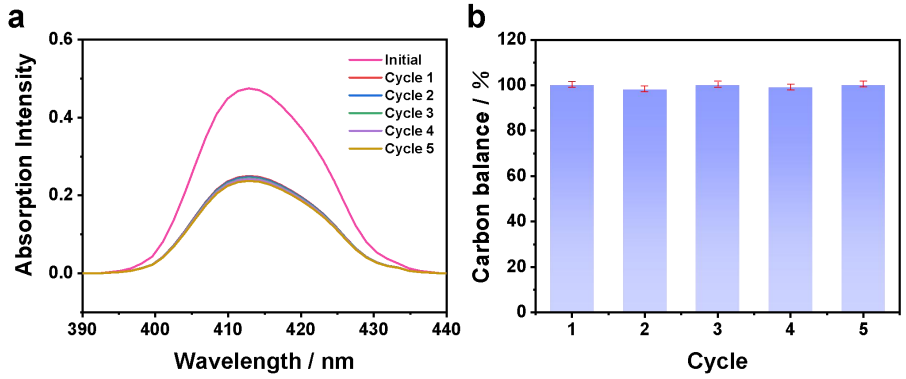

Figure S23. (a) UV-vis absorption spectra of the testing solution containing acetyl acetone solution and the anolyte before and post per electrolysis cycle. (b) Carbon balance of HCHO oxidation in per electrolysis cycle. Error bars represent the standard deviation of at least three independent measurements.

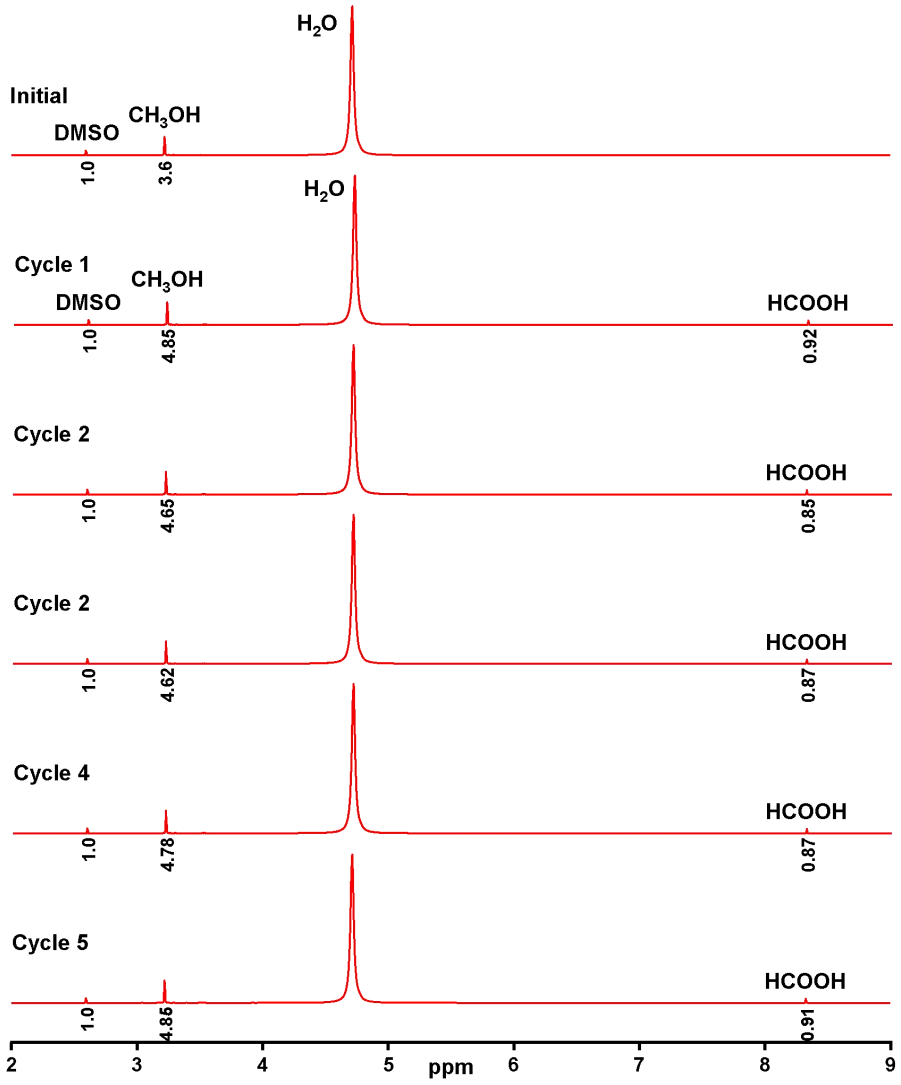

Figure S24. The ^{1}H NMR (D_2O, 400 MHz) of organic products in the liquid phase of the anode chamber at five consecutive 1 h controlled-current density electrolysis (500 mA cm^{-2}) in a two-electrode electrolyzer using the Cu_3Ag_7/CF and Cu_7Ag_3/CF couple but fresh electrolyte for each cycle.

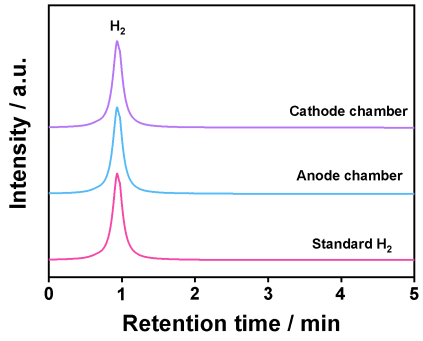

Figure S25. The GC of gas products collected from each cathode and anode chamber in a two-electrode electrolyzer consisting of Cu_3Ag_7/CF anode and Cu_7Ag_3/CF cathode at a cell voltage of 0.5 V, in which 1.0 M KOH and 0.05 M FF as the catholyte and 1.0 M KOH and 0.6 M HCHO as the anolyte.

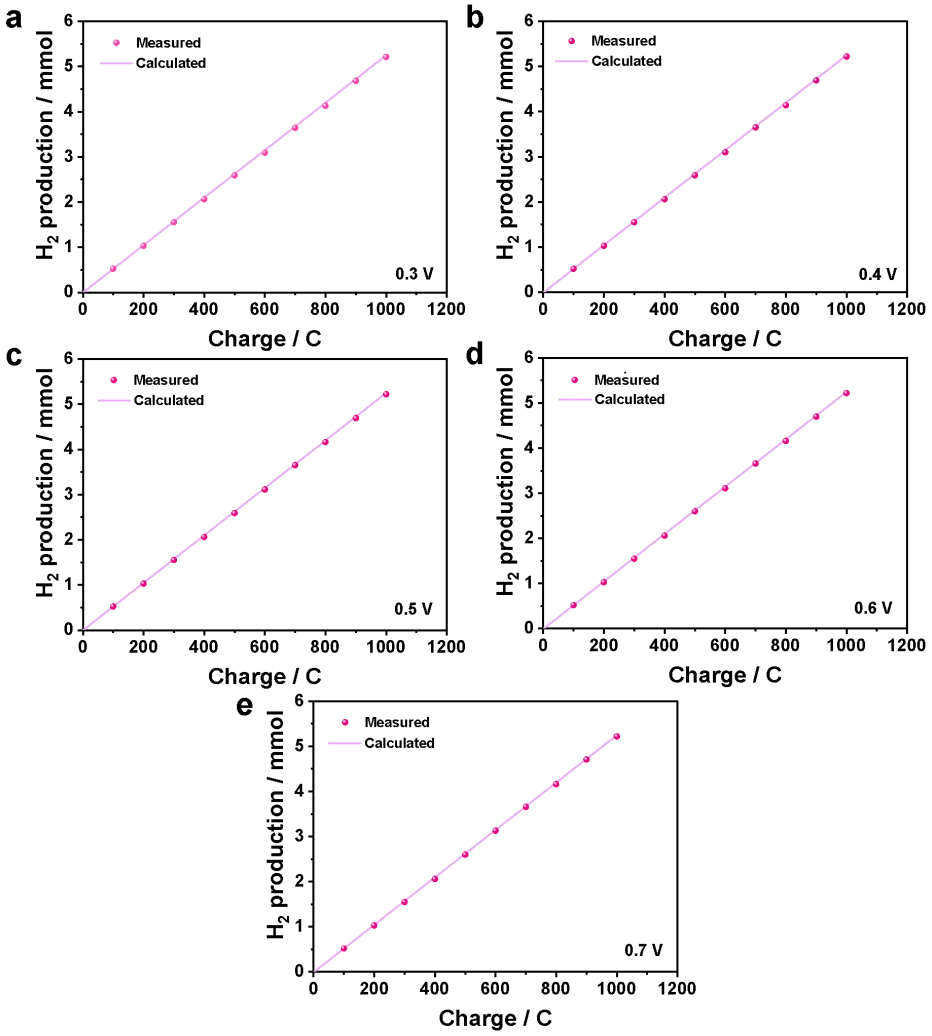

Figure S26. (a-e) Comparison of the experimentally measured H_2 amounts with the theoretical H_2 amounts along the passed charge for the anode chambers during each electrolysis with different voltage inputs (0.3 ~ 0.7 V) in a two-electrode electrolyzer consisting of Cu_3Ag_7/CF anode and Cu_7Ag_3/CF cathode, in which 1.0 M KOH and 0.05 M FF as the catholyte and 1.0 M KOH and 0.6 M HCHO as the anolyte.

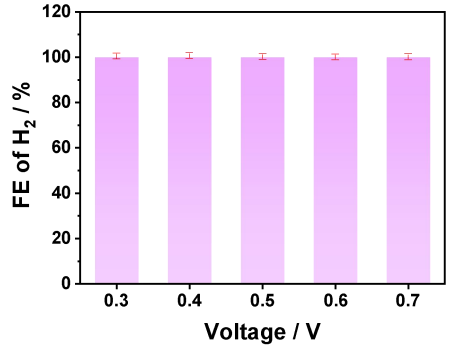

Figure S27. FE of H_2 in the anode chamber at different voltage inputs.

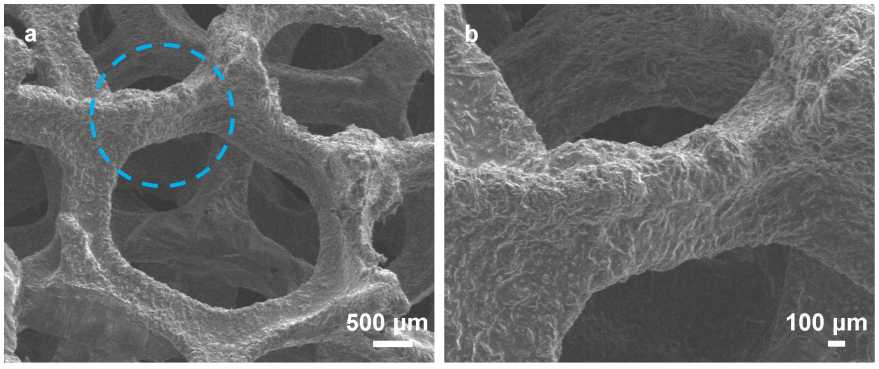

Figure S28. (a) (b) SEM of the Cu_7Ag_3/CF after a reaction at a cell voltage of 0.6 V in a two-electrode electrolyzer electrolyzer consisting of Cu_3Ag_7/CF anode and Cu_7Ag_3/CF cathode, in which 1.0 M KOH and 0.05 M FF solution as the catholyte and 1.0 M KOH and 0.6 M HCHO solution as the anolyte.

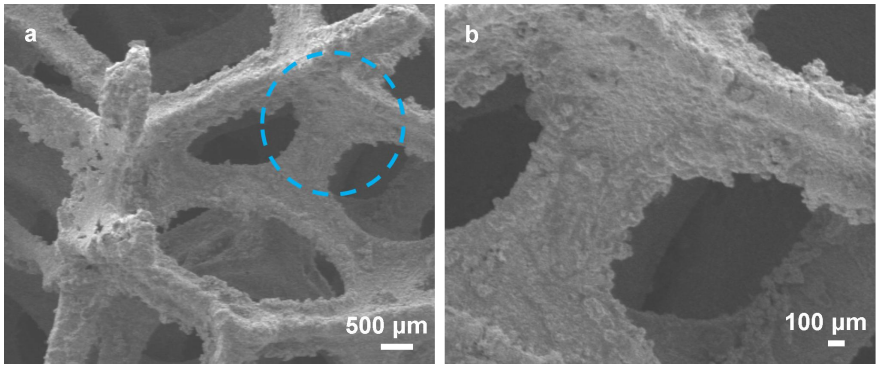

Figure S29. (a) (b) SEM of the Cu_3Ag_7/CF after a reaction at a cell voltage of 0.6 V in a two-electrode electrolyzer electrolyzer consisting of Cu_3Ag_7/CF anode and Cu_7Ag_3/CF cathode, in which 1.0 M KOH and 0.05 M FF solution as the catholyte and 1.0 M KOH and 0.6 M HCHO solution as the anolyte.

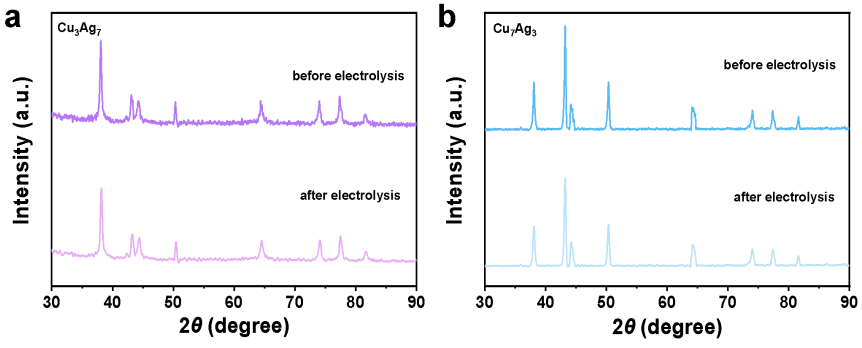

Figure S30. XRD patterns before and post electrolysis. (a) Cu_3Ag_7. (b) Cu_7Ag_3.

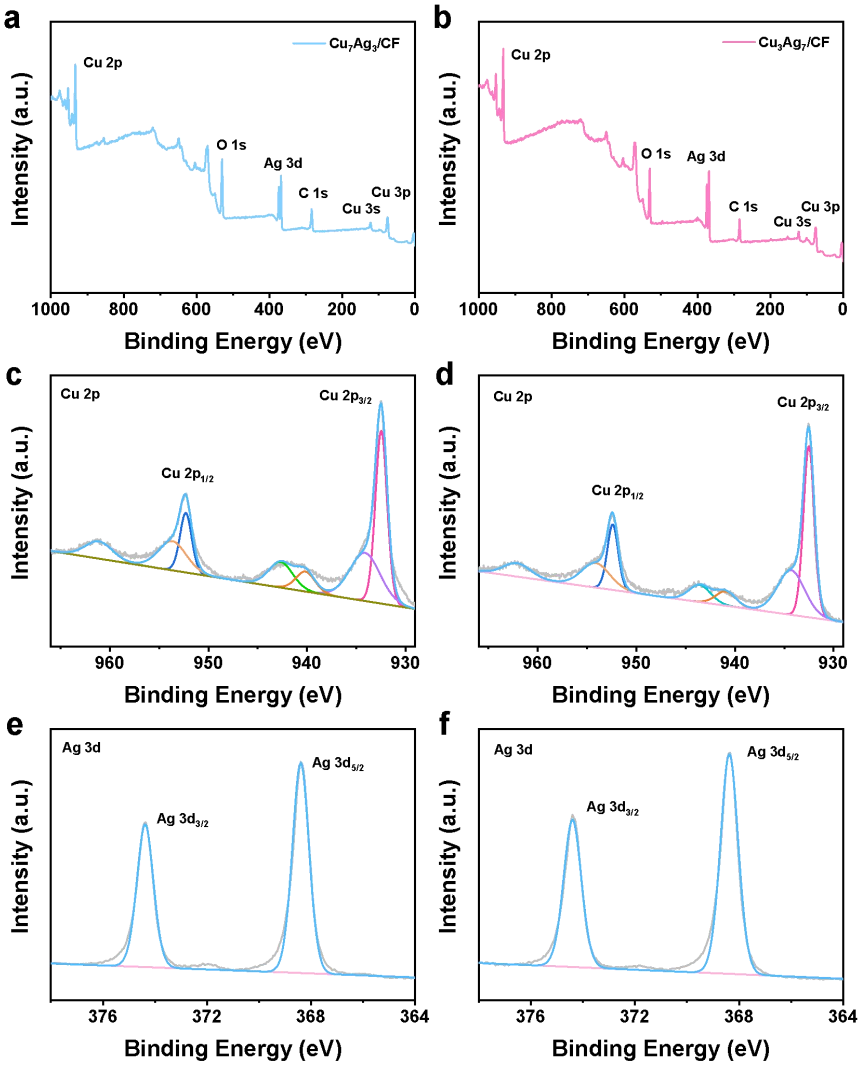

Figure S31. High-resolution XPS spectra of Cu_7Ag_3/CF and Cu_3Ag_7/CF. (a) XPS measurement spectrum of Cu_7Ag_3/CF. High resolution XPS spectra of Cu_7Ag_3/CF (c) Cu 2p (e) Ag 3d. (b) XPS measurement spectrum of Cu_3Ag_7/CF. High resolution XPS spectra of Cu_3Ag_7/CF (d) Cu 2p (f) Ag 3d.

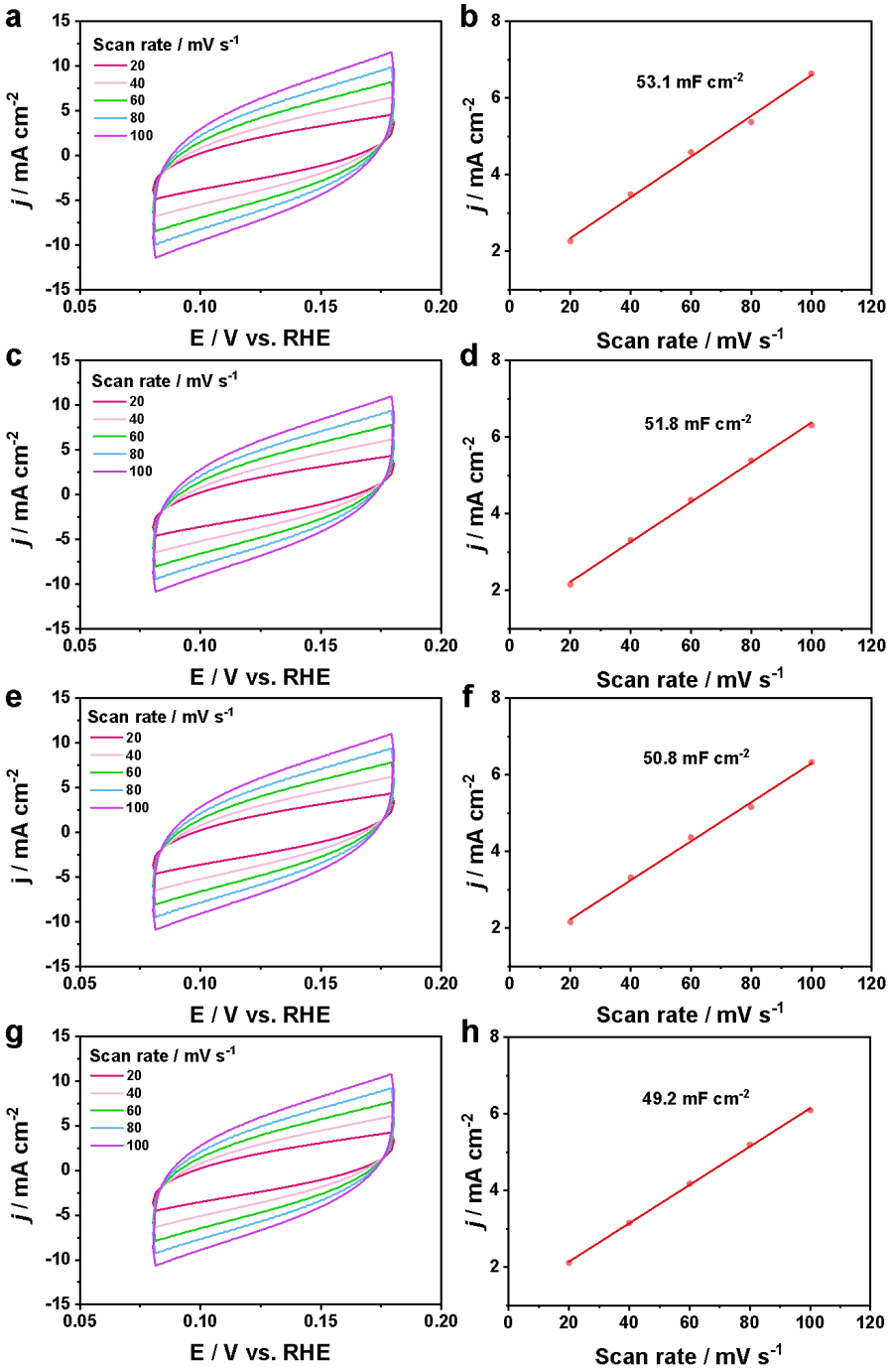

Figure S32. CV curves of Cu_7Ag_3/CF (a, c) and Cu_3Ag_7/CF (e, g) before and after chronoamperometric experiment were collected in a non-Faradaic region with various scan rates ranging from 20 to 100 mV s^{-1} at potentials between 0.08 V and 0.18 V vs RHE in 1.0 M KOH solution under an Ar atmosphere. C_{dl} values of Cu_7Ag_3/CF electrode (b) before and (d) after chronoamperometric experiment. C_{dl} values of Cu_3Ag_7/CF electrode (f) before and (h) after chronoamperometric experiment.

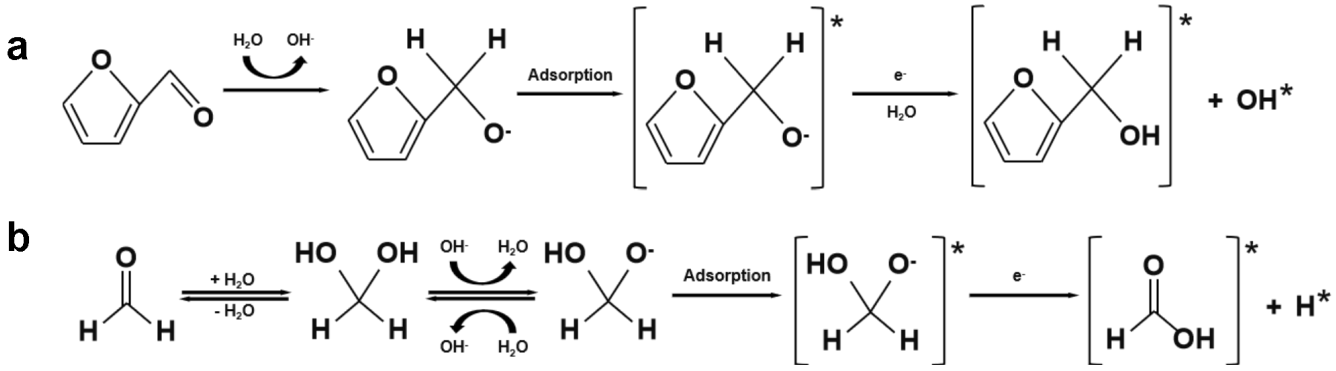

Figure S33. Reaction path. (a) Proposed mechanism from FF reduced to FA. (b) Proposed mechanism from HCHO oxidation to HCOOH.

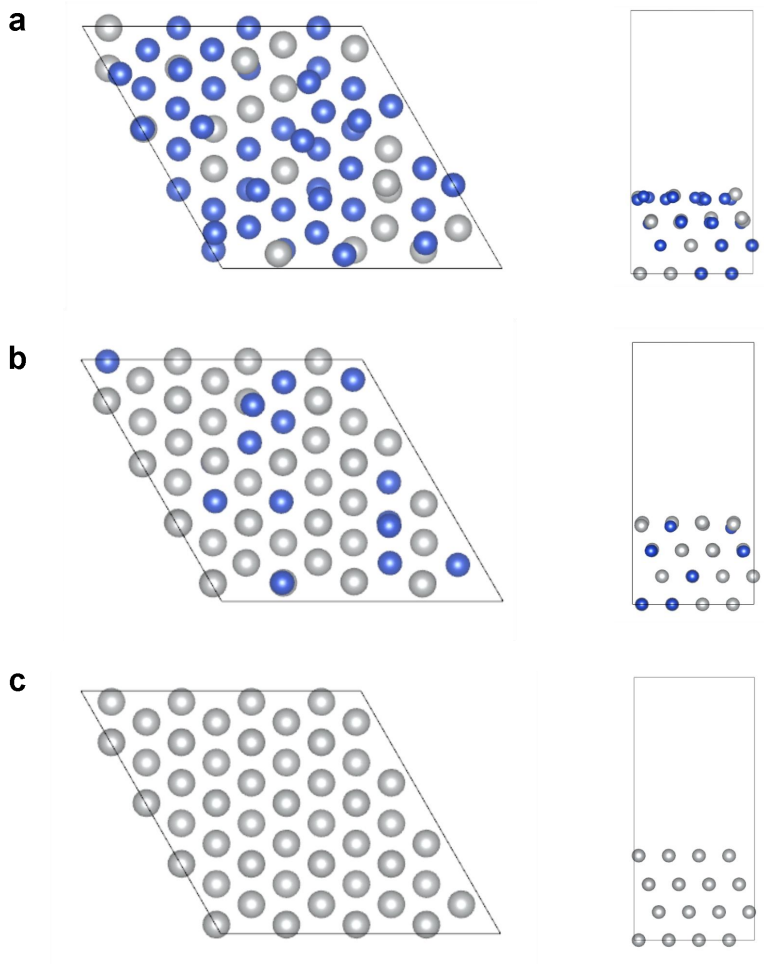

Figure S34. Models of the (111) surfaces of (a) Cu_7Ag_3, (b) Cu_3Ag_7, and (c) Ag (Cu is the same as model Ag, sharing the same one model).

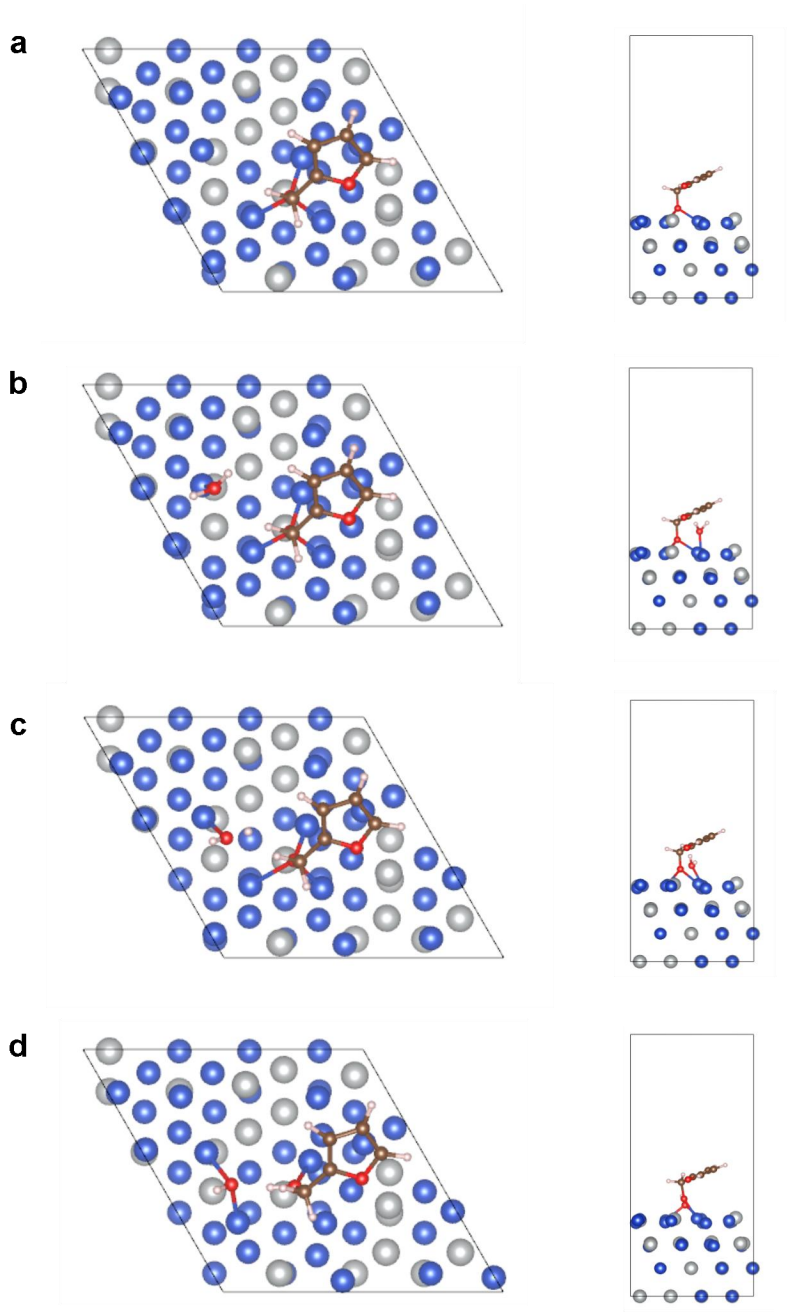

Figure S35. Computational models of Cu_7Ag_3. Optimized geometry of adsorbed (a) $(C_4H_3O)CH_2O$, (b) $(C_4H_3O)CH_2O$ and H_2O, (c) $(C_4H_3O)CH_2O$ and H_2O and (d) $(C_4H_3O)CH_2OH$ and OH* on the surface. Top view (left side) and side view (right side). (Red: O, Pink: H, Brown: C, Blue: Cu, Gray: Ag)

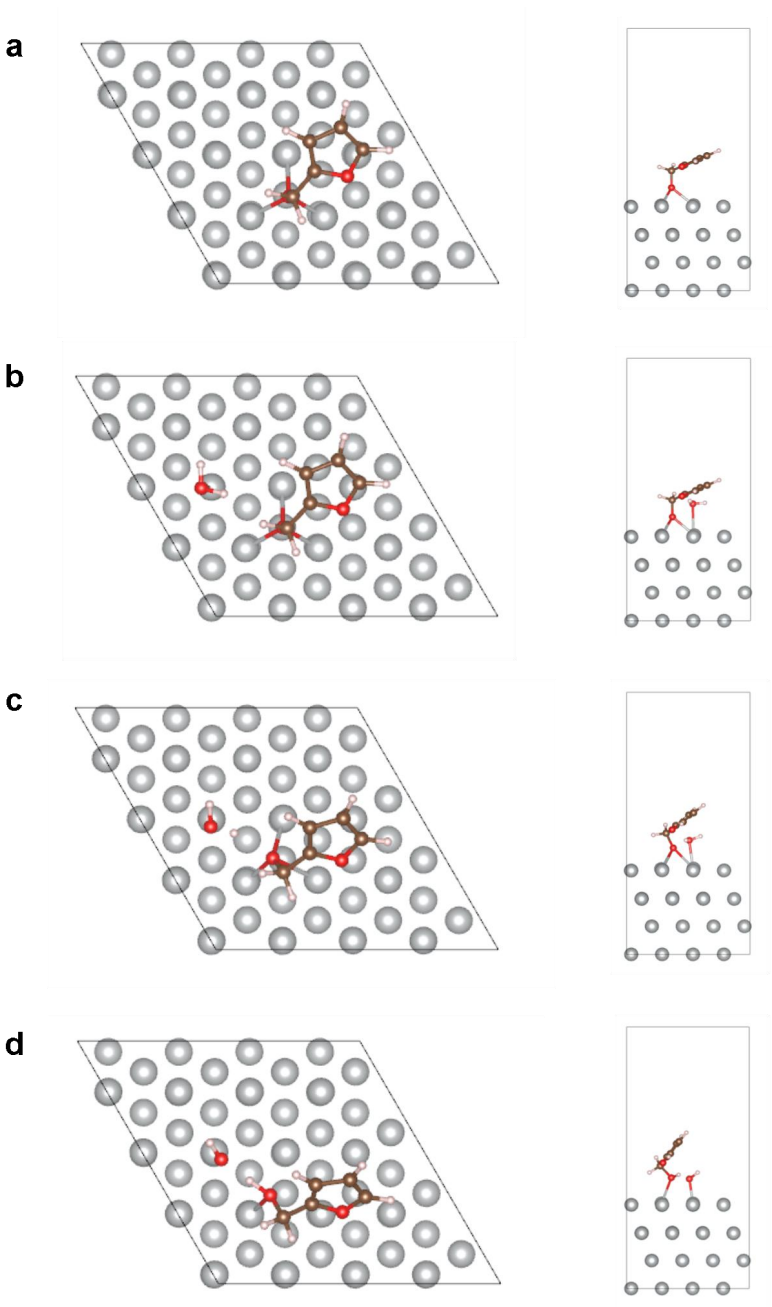

Figure S36. Computational models of Cu. Optimized geometry of adsorbed (a) $(C_4H_3O)CH_2O$, (b) $(C_4H_3O)CH_2O$ and H_2O, (c) $(C_4H_3O)CH_2O$ and H_2O and (d) $(C_4H_3O)CH_2OH$ and OH* on the surface. Top view (left side) and side view (right side). (Red: O, Pink: H, Brown: C, Gray: Cu)

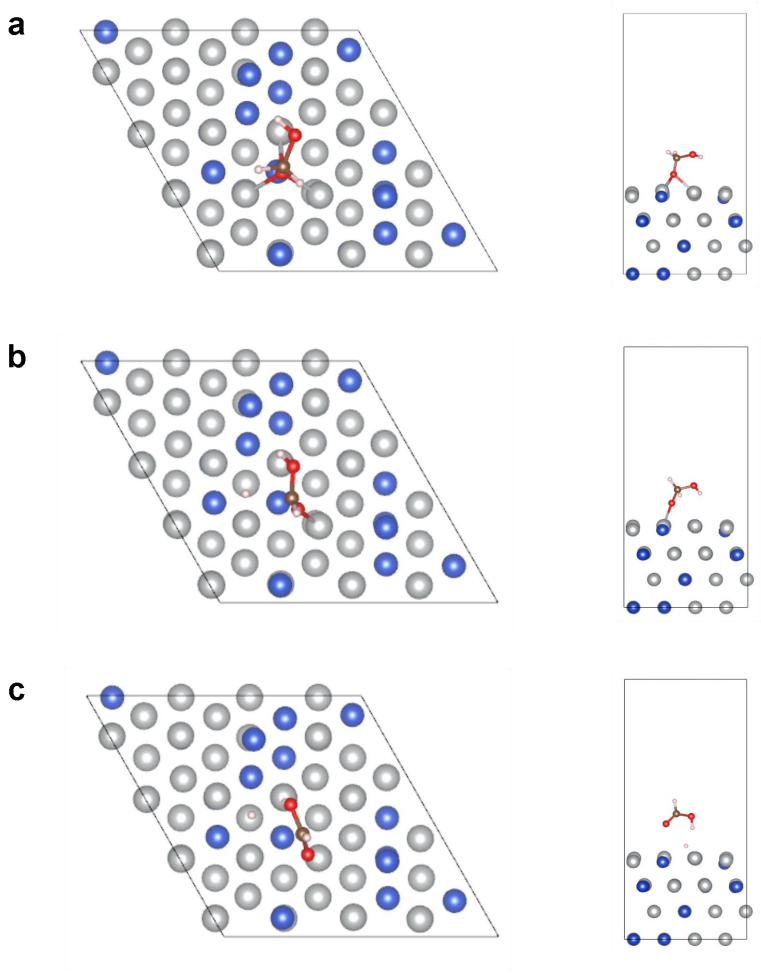

Figure S37. Computational models of Cu_3Ag_7. Optimized geometry of adsorbed (a) $H_2C(OH)O$, (b) $H_2C(OH)O$ stripped of H and (c) HCOOH and H* on the surface. Top view (left side) and side view (right side). (Red: O, Pink: H, Brown: C, Blue: Cu, Gray: Ag)

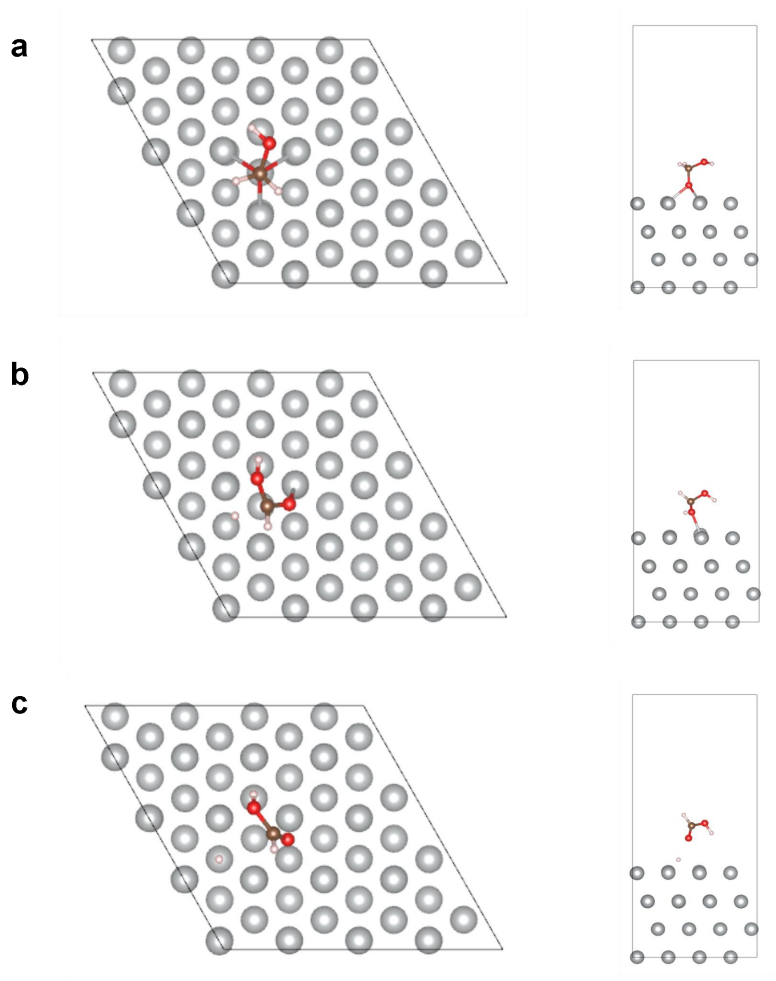

Figure S38. Computational models of Ag. Optimized geometry of adsorbed (a) $H_2C(OH)O$, (b) $H_2C(OH)O$ stripped of H and (c) HCOOH and H* on the surface. Top view (left side) and side view (right side). (Red: O, Pink: H, Brown: C, Gray: Ag)

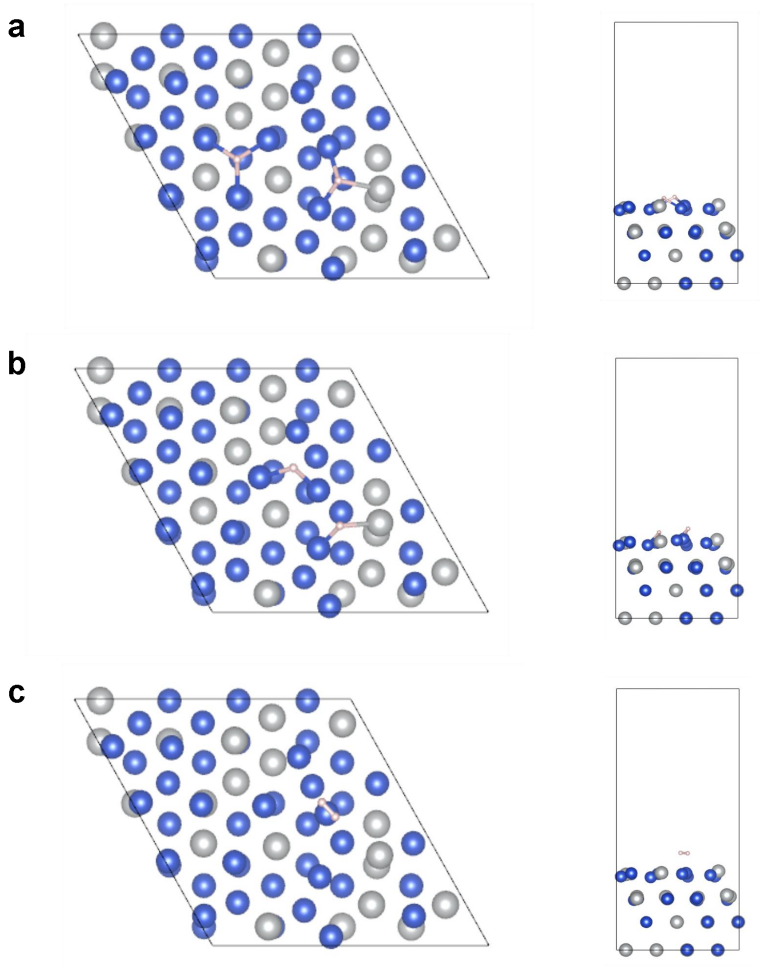

Figure S39. Computational models of Cu_7Ag_3. Optimized geometry of adsorbed (a) H*, (b) H_2 formation from H* and (c) H_2 on the surface. Top view (left side) and side view (right side). (Pink: H, Blue: Cu, Gray: Ag)

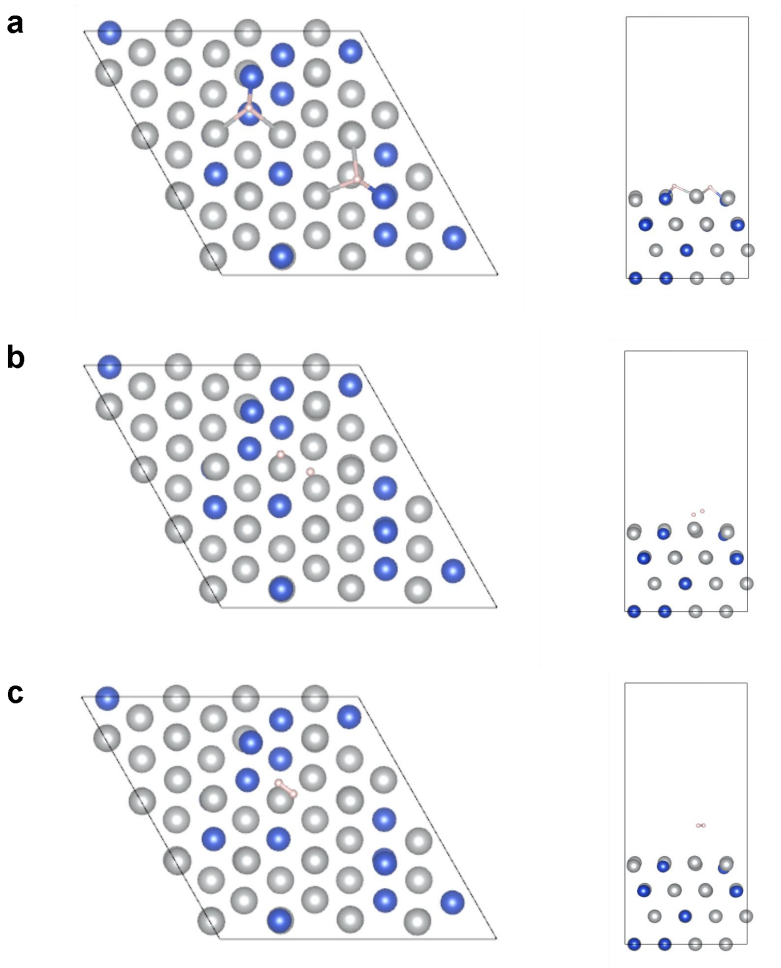

Figure S40. Computational models of Cu_3Ag_7. Optimized geometry of adsorbed (a) H*, (b) H_2 formation from H* and (c) H_2 on the surface. Top view (left side) and side view (right side). (Pink: H, Blue: Cu, Gray: Ag)

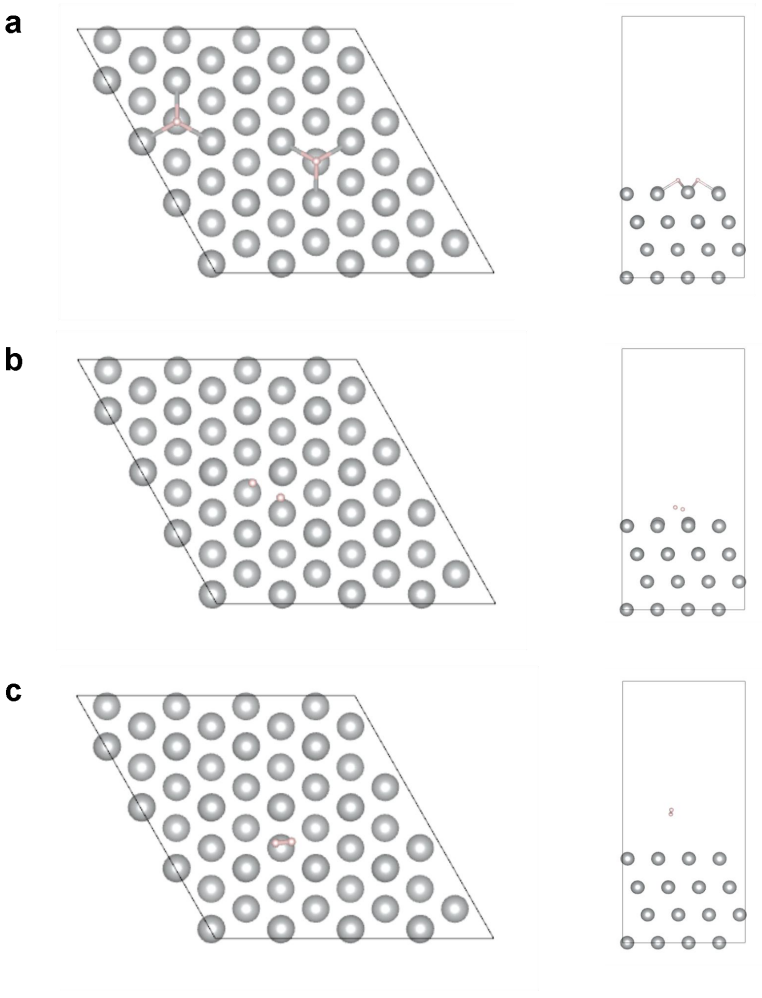

Figure S41. Computational models of Ag (Cu). Optimized geometry of adsorbed (a) H*, (b) H_2 formation from H* and (c) H_2 on the surface. Top view (left side) and side view (right side). (Pink: H, Gray: Ag (Cu))

Table S1. Atomic ratios of Cu_xAg_y characterized by ICP-AES.

Catalyst	Cu atom%	Ag atom%
Cu_1Ag_9	9.8	90.2
Cu_3Ag_7	29.4	70.6
Cu_5Ag_5	50.1	49.9
Cu_7Ag_3	69.5	30.5
Cu_9Ag_1	89.1	10.9

Table S2. Atomic ratios Cu_xAg_y were characterized by XPS results.

Catalyst	Cu atom%	Ag atom%
Cu_1Ag_9	11.2	88.8
Cu_3Ag_7	30.6	69.4
Cu_5Ag_5	49.3	50.7
Cu_7Ag_3	69.9	30.1
Cu_9Ag_1	90.4	9.6

Table S3. The FE of the anode products were calculated from the amount of H_2 and organic products at different voltages in the two-electrode electrolyzer.

Voltage	n_{HCOOH} (mmol)		n_{CH_3OH} (mmol)	n_{HCOO^-} (mmol)	FE_{HCOO^-}	n_{H_2} (mmol)	FE_{H_2}
	From HCHO Electrooxidation	From Cannizzaro reaction	From Cannizzaro reaction				
0.3 V	4.98	2.98	2.98	5.01	100%	2.49	100%
0.4 V	5.05	3.15	3.15	5.09	100%	2.53	100%
0.5 V	5.01	2.86	2.86	5.02	100%	2.50	100%
0.6 V	5.06	3.23	3.23	5.12	100%	2.55	100%
0.7 V	5.10	3.18	3.18	5.15	100%	2.57	100%

***Condition**: Electrolysis was carried out in a two-electrode electrolyzer using Cu_3Ag_7/CF and Cu_7Ag_3/CF pairs at different voltages, with a new electrolyte at each voltage, where 1.0 M KOH and 0.05 M FF were used as the cathodic solution and 1.0 M KOH and 0.6 M HCHO were used as the anodic solution.

Table S4. The FE of anodic products and carbon balance based on the amounts of H_2 and organic products during each electrolysis in a two-electrode electrolyzer.

Entry	n_{HCOOH} (mmol)		n_{CH_3OH} (mmol)	n_{HCOO^-} (mmol)	FE_{HCOO^-}	n_{H_2} (mmol)	FE_{H_2}	n_{HCHO} (mmol)	Carbon balance
	From HCHO Electroo-xidation	From Cannizzaro reaction	From Cannizzaro reaction						
Cycle 1	5.18	3.12	3.12	5.18	100%	5.20	200%	16.52	100%
Cycle 2	5.12	3.06	3.06	5.10	100%	5.10	200%	16.40	98%
Cycle 3	5.10	28.6	28.6	5.09	100%	5.10	200%	16.32	97%
Cycle 4	5.01	3.58	3.58	5.02	100%	5.05	200%	16.42	100%
Cycle 5	4.89	3.33	3.33	4.9	100%	5.00	200%	16.61	100%

***Condition**: Five consecutive 1 h controlled-current density electrolysis (500 mA cm^{-2}) were carried out in a two-electrode electrolyzer using Cu_3Ag_7/CF and Cu_7Ag_3/CF pairings, with fresh electrolyte used for each cycle, where 1.0 M KOH and 0.05 M FF were the cathodic solution, and 1.0 M KOH and 0.6 M HCHO were the cathodic solution.

Table S5. Assignments of the vibration bands observed on the in-situ FTIR spectra in 1.0 M KOH and 0.05 M FF recorded on Cu_7Ag_3/CF.

Vibration band (cm^{-1})		Compound	Assignment
Positive	Negative		
1684		FF	C=O stretching
1670		FF	C=O stretching
1566		FF	C=C of furan cycle stretching
1475		FF	C=C stretching, furan ring bending
1393		FF	CH aldehyde bending, C=O stretching
1277		FF	C-O stretching, C-C aldehyde stretching, furan ring bending, CH aldehyde bending
	1502	FA	Furan ring C=C stretching
	1217	FA	Furan ring stretching, C-O stretching, ring-CH_2 stretching
	1144	FA	Furan ring, collective vibration
	1006	FA	Furan ring stretching, CH ring bending
	967	FA	Furan ring, collective vibration

Table S6. A comparison of electrolysis performance of inorganic and organic feedstocks electrooxidation integrated with electroreduction in two-electrodes electrolyzer.

Oxidation substrates	Reduction Substrate	Catalysts	product	Current density (mA cm^{-2})	Cell voltage (V)	Ref.
HCHO	Furfural	Cu_3Ag_7/CF(+)|| Cu_7Ag_3/CF(–)	Furfuryl alcohol, Formate, H_2	500	0.5	This work
HCHO	H_2O	Cu_3Ag_7/CF(+)|| Ni_3N/Ni/NF(–)	Formate, H_2	500	0.6	1
HMF	CO_2	InOOH-O_V (+, –)	FDCA, HCOOH	10	2.27	2
H_2O	CO_2	Zn/SnO_2 (+, –)	H_2O_2, $HCOO^-$	100	3.8	3
HCHO	NO_3^-	Cu_2O(+, –)	HCOOH, NH_4^+	10	0.56	4
Cellulose	H_2O	$H_6[PV_3Mo_9O_{40}]$ (+)||Pt(–)	Formic acid, H_2	50	1.22	5
Glucose	H_2O	$NiFeO_x$-NF(+)||$NiFeN_x$-NF(–)	Glucaric acid, H_2	200	1.48	6
Na_2S	H_2O	CoS_2@C/MXene/NF(+)||CoO@C/MXene/NF (–)	Sulfur, H_2	300	0.97	7
1,3-propan-ediol	H_2O	PdBi/NF(+)||Pt(–)	3-Hydroxypropionic acid, H_2	20	0.86	8
Glycerol	H_2O	$NiCo_2O_4$/NF(+)|| Ni(–)	Formate, H_2	10	1.35	9

References

1 G. Li, G. Han, L. Wang, X. Cui, N. K. Moehring, P. R. Kidambi, D.-e. Jiang and Y. Sun, *Nat. Commun.*, 2023, **14**, 525.

2 F. Ye, S. Zhang, Q. Cheng, Y. Long, D. Liu, R. Paul, Y. Fang, Y. Su, L. Qu, L. Dai and C. Hu, *Nat. Commun.*, 2023, **14**, 2040.

3 X. Hu, G. Mei, X. Chen, J. Liu, B. Y. Xia and B. You, *Angew. Chem. Int. Ed.*, 2023, **62**, e202304050.

4 L. Xiao, W. Dai, S. Mou, X. Wang, Q. Cheng and F. Dong, *Energy Environ. Sci.*, 2023, **16**, 2696-2704.

5 W. Tang, L. Zhang, T. Qiu, H. Tan, Y. Wang, W. Liu and Y. Li, *Angew. Chem. Int. Ed.*, 2023, **62**, e202305843.

6 W. Liu, Z. Xu, D. Zhao, X. Pan,H. Li, X. Hu, Z. Fan, W. Wang, G. Zhao, S. Jin, G. W. Huber and H. Yu, *Nat. Commun.*, 2020, **11**, 265.

7 L. Zhang, Z. Wang and J. Qiu, *Adv. Mater.*, 2022, **34**, 2109321.

8 D. Si, M. Wang, X. Yang, C. Wang, K. Shi, B. Huang, L. Chen and J. Shi, *Appl. Catal. B Environ.*, 2023, **331**, 122664.

9 G. Wu, X. Dong, J. Mao, G. Li, C. Zhu, S. Li, A. Chen, G. Feng, Y. Song, W. Chen and W. Wei, *Chem. Eng. J.*, 2023, **468**, 143640.